Title: Distinct CD3$^+$ CD14$^+$ T Cell-Monocytes are dynamic complexes that harbor HIV and are increased with glucose intolerance

Authors: Celestine N. Wanjalla[1†], Joshua Simmons[1], Jared Oakes[1,2], Xiuqi Zhang[1], Cindy Nochowicz[1], Stephen Priest[1], Samuel S. Bailin[1], Christopher M. Warren[3], Mona Mashayekhi[4], Heather K. Beasley[5], Jian Wang[6], Leslie Meenderink[1,3], Quanhu Sheng[7], Joey Stolze[7], Rama Gangula[1], Abha Chopra[8], Curtis L. Gabriel[9], Tecla Temu[10], Suman Pakala[1], Erin M. Wilfong[11,12], Sara Gianella[13], Elizabeth J. Phillips[1,8,12], David G. Harrison[14], Antentor Hinton[5] ,Spyros A. Kalams[1,2], Simon A. Mallal[1,8,15], John R. Koethe[1,3]

[1]Division of Infectious Diseases, Vanderbilt University Medical Center, Nashville, TN, USA

[2] Department of Pathology, Microbiology, and Immunology, Vanderbilt University Medical Center, Nashville, Tennessee, USA

[3] Veterans Affairs Tennessee Valley Healthcare System, Nashville, TN

[4] Division of Diabetes, Endocrinology, and Metabolism, Vanderbilt University Medical Center, Nashville, TN, USA

[5] Department of Molecular Physiology and Biophysics, Vanderbilt University, Nashville, TN, USA

Department of Pathology, Microbiology, and Immunology, Vanderbilt University Medical Center, Nashville, Tennessee, USA

[6] Central Microscopy Research Facility, University of Iowa, Iowa City, IA

[7] Department of Biostatistics, Vanderbilt University, Nashville, TN, USA

[8] Institute for Immunology and Infectious Diseases, Murdoch University, Murdoch, WA, Australia

[9] Division of Gastroenterology, Vanderbilt University Medical Center, Nashville, TN, USA

[10] Departments of Global Health, University of Washington, Seattle, WA, USA

[11] Division of Rheumatology and Immunology, Vanderbilt University Medical Center, Nashville, TN, USA

27 [12] Division of Allergy, Pulmonary, and Critical Care Medicine, Vanderbilt University Medical
28 Center, Nashville, TN, USA
29 [13] Department of Medicine, University of California, San Diego, CA, USA
30 [14] Division of Clinical Pharmacology, Vanderbilt University Medical Center, Nashville, TN, USA
31 [15] Department of Biomedical Informatics, Vanderbilt University, Nashville, TN, USA
32
33 [†] Corresponding author: Celestine N. Wanjalla, MD, Ph.D.; Division of Infectious Diseases,
34 Vanderbilt University Medical Center, A-2200 MCN, 1161 21st Ave S., Nashville, TN, 37232-
35 2582. (615) 322-2035 (o), (615) 343-6160 (f), celestine.wanjalla@vumc.org
36
37 Abstract word count: 153
38 Main text word count: 8901
39 Tables and Figures: 7
40 Supplemental tables and figures: 14
41 Videos: 2
42
43 Running Title (50 characters): $CD3^+CD14^+$ complexes higher in HIV+ with diabetes
44 Keywords (5): HIV, immune complexes, doublets, diabetes, reservoir
45

Summary

Persistent systemic inflammation in persons with HIV (PWH) is accompanied by an increased risk of metabolic disease. Yet, changes in the innate and adaptive immune system in PWH who develop metabolic disease remain poorly defined. Using unbiased approaches, we show that PWH with prediabetes/diabetes have a significantly higher proportion of circulating $CD14^+$ monocytes complexed to T cells. The complexed $CD3^+$ T cells and $CD14^+$ monocytes demonstrate functional immune synapses, increased expression of proinflammatory cytokines, and greater glucose utilization. Furthermore, these complexes harbor more latent HIV DNA compared to $CD14^+$ monocytes or $CD4^+$ T cells. Our results demonstrate that circulating $CD3^+CD14^+$ T cell-monocyte pairs represent functional dynamic cellular interactions that likely contribute to inflammation and, in light of their increased proportion, may have a role in metabolic disease pathogenesis. These findings provide an incentive for future studies to investigate T cell-monocyte immune complexes as mechanistic in HIV cure and diseases of aging.

61 **Graphical Abstract**

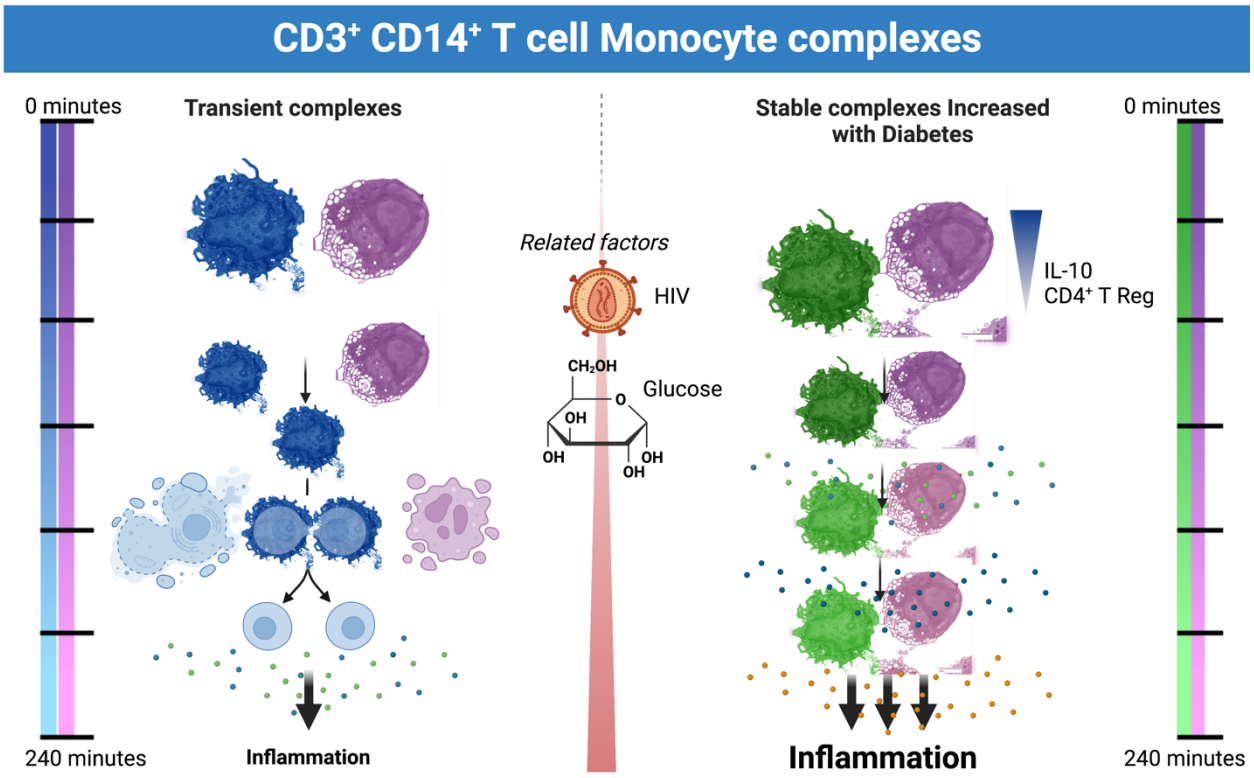

62

63 **Highlights**

64 • Persons with HIV and diabetes have increased circulating $CD3^+$ $CD14^+$ T cell-monocyte
65 complexes.
66 • $CD3^+$ $CD14^+$ T cell-monocytes are a heterogenous group of functional and dynamic
67 complexes.
68 • We can detect HIV in T cell-monocyte complexes.
69 • The proportion of $CD3^+$ $CD14^+$ T cell-monocyte complexes is positively associated with
70 blood glucose levels and negatively with plasma IL-10 and $CD4^+$ T regulatory cells.

71

Introduction

Persons with HIV (PWH) on antiretroviral therapy often have heightened, chronic inflammation that may contribute to age-related diseases such as diabetes and atherosclerosis.[1-8] This increased risk of age-related diseases offers an opportunity to investigate how inflammation contributes to the development of cardiometabolic disorders. [9] We used unbiased approaches to comprehensively characterize alterations in immune cell populations that distinguish PWH with prediabetes or diabetes from those with HIV alone.

Common flow cytometry analysis workflows may overlook interacting cell populations. Typically, presumed single cells suspensions in droplets of buffered fluid are illuminated by the laser beam to capture cell marker expression. During analysis, steps are taken to eliminate cell aggregates which have commonly been presumed to arise ex-vivo due to cell clumping via adhesion molecules and other factors introduced during sample processing, particles on dying cells, or lack of separation of cells due to high-stream flow rates. [10] [11,12] Recent studies, however, have demonstrated the existence of immunologically relevant cell-cell complexes in the blood of individuals with immune perturbation due to infection, vaccination, and cancer. [13,14] [15] Burel *et. al.* found that the presence of $CD3^+$ T cell - $CD14^+$ monocyte complexes in freshly isolated blood was strongly correlated with their presence in cryopreserved peripheral blood mononuclear cells (PBMCs), suggesting that their occurrence in cryopreserved PBMCs is not an artifact of processing or storage. [13] The reorganization of adhesion molecules at the immunological synapse between the monocyte and the T cells indicated an activating interaction between these cells. [13] Similar T-cell complexes have been observed with antigen-presenting B cells. [16,17]

In the context of HIV, the ineffective killing of HIV-infected macrophages by cytotoxic T lymphocytes may lead to prolonged immunologic synapses resulting in greater inflammation due to the secretion of cytokines and chemokines. [18] The hypothesis is supported by a similar

98 phenomenon in diseases such as familial hemophagocytic lymphohistiocytosis, where
99 lymphocytes engage but fail to kill myeloid cells, which leads to prolonged expression of
100 proinflammatory cytokines and an elevated systemic inflammatory response. [19]
101
102 PWH have chronic systemic inflammation which persists despite effective suppression of
103 plasma viremia on treatment and is thought to contribute to the development of diabetes and
104 metabolic disease more broadly. Furthermore, once PWH develop diabetes, the altered immune
105 responses in the context of continued hyperglycemia may create a reinforcing cycle that leads
106 to further inflammation and greater metabolic dysregulation. To investigate these relationships
107 further, we used unbiased analyses to investigate alterations in immune factors in the presence
108 and absence of glucose intolerance in PWH.

Results

Descriptive characteristics of the cohort

The study cohort was comprised of 38 participants with HIV on antiretroviral therapy with long-term suppression of plasma viremia: 14 without diabetes (hemoglobin A1c [HbA1c] <5.7% and fasting blood glucose [FBG] <100 mg/dl), and 24 with prediabetes (HbA1c 5.7-6.4% and/or FBG 100-125 mg/dl) or diabetes (HbA1c ≥6.5%, FBG≥126 mg/dl and/or on anti-diabetic medication) (**Table S1**). Individuals with prediabetes and diabetes were combined into a single metabolic disease group. The clinical characteristics of the participants were largely similar, except for parameters linked to glucose intolerance such as body mass index ($p<0.05$), waist and hip circumference ($p<0.05$, $p=0.01$ respectively), and fasting blood sugar ($p<0.001$). Individuals without glucose intolerance were younger (median age 39 [IQR 35, 53] versus 49 [IQR 40, 56]), but this difference did not reach statistical significance ($p=0.1$). There were no notable differences observed in the HIV-related laboratory values or antiretroviral therapy regimens.

Circulating cells of the innate and adaptive immune system differ by metabolic health in PWH

Mass cytometry was used to examine immune cells in cryopreserved peripheral blood mononuclear cells (PBMCs) of all participants (**Figure S1A**). We identified six primary clusters including $CD4^+$ T cells, senescent $CD4^+$ T cells (termed 'CGC$^+$' cells due to co-expression of CX3CR1, GPR56, and CD57 surface markers[20]), $CD8^+$ T cells, monocytes, B cells, and NK cells (**Figure 1A**). A comparison of clusters (abundance/size differences) between individuals with diabetes, prediabetes, and those without revealed several clusters in participants with glucose intolerance that were apparently fewer in PWH without diabetes depicted with the red dotted circles, all $p<0.05$ (**Figure 1B, Figure S1B**). Other cell types in the blue clusters that were more abundant in PWH without diabetes included classical monocytes, $CD8^+$ naïve T cells, $\gamma\delta$ T cells,

135 memory B cells, $CD4^+$ T regulatory cells, and $CD14^+$ $CD16^{+/-}$ Monocytes (**Table S2**). The
136 heatmap represents the relative expression (median) of the surface immune markers on cells
137 and the median fold difference in cluster sizes. Magenta clusters were more abundant in
138 prediabetic/diabetic PWH, whereas blue clusters were more abundant in non-diabetic PWH
139 (**Figure 1C**). CGC^+ $CD4^+$ T cells, a population we have previously reported as associated with
140 both metabolic and cardiovascular disease conditions in treated HIV, were also increased with
141 diabetes. [2,20,21]
142
143

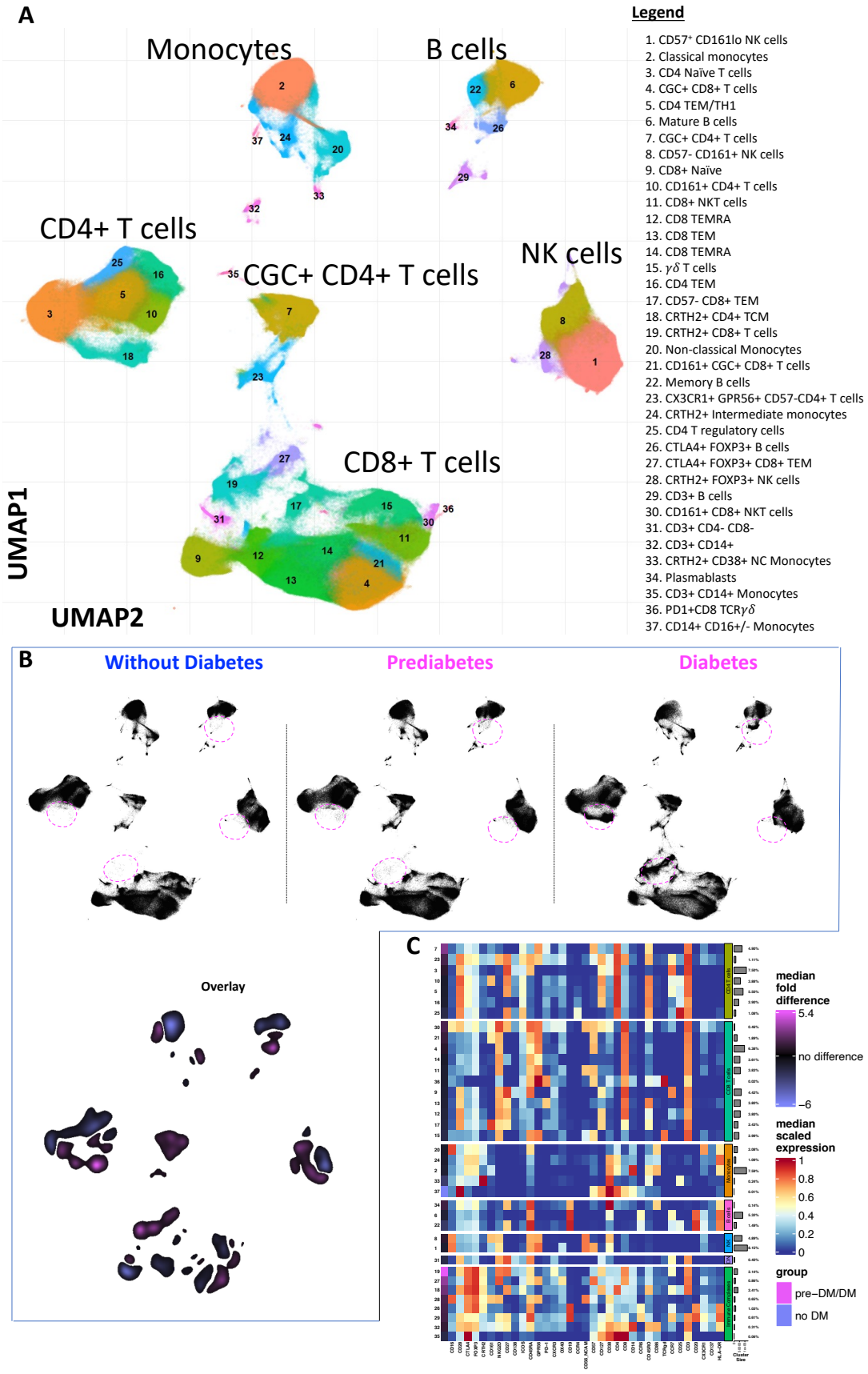
A
Monocytes
B cells
CD4+ T cells
CGC+ CD4+ T cells
NK cells
CD8+ T cells
UMAP1
UMAP2
Legend
1. CD57+ CD161lo NK cells
2. Classical monocytes
3. CD4 Naïve T cells
4. CGC+ CD8+ T cells
5. CD4 TEM/TH1
6. Mature B cells
7. CGC+ CD4+ T cells
8. CD57- CD161+ NK cells
9. CD8+ Naïve
10. CD161+ CD4+ T cells
11. CD8+ NKT cells
12. CD8 TEMRA
13. CD8 TEM
14. CD8 TEMRA
15. γδ T cells
16. CD4 TEM
17. CD57- CD8+ TEM
18. CRTH2+ CD4+ TCM
19. CRTH2+ CD8+ T cells
20. Non-classical Monocytes
21. CD161+ CGC+ CD8+ T cells
22. Memory B cells
23. CX3CR1+ GPR56+ CD57-CD4+ T cells
24. CRTH2+ Intermediate monocytes
25. CD4 T regulatory cells
26. CTLA4+ FOXP3+ B cells
27. CTLA4+ FOXP3+ CD8+ TEM
28. CRTH2+ FOXP3+ NK cells
29. CD3+ B cells
30. CD161+ CD8+ NKT cells
31. CD3+ CD4- CD8-
32. CD3+ CD14+
33. CRTH2+ CD38+ NC Monocytes
34. Plasmablasts
35. CD3+ CD14+ Monocytes
36. PD1+CD8 TCRγδ
37. CD14+ CD16+/- Monocytes
B
Without Diabetes
Prediabetes
Diabetes
Overlay
C
median fold difference
5.4
no difference
−6
median scaled expression
1
0.8
0.6
0.4
0.2
0
group
pre−DM/DM
no DM

144

Figure 1. Phenotypic characterization of PBMCs in non-diabetic, prediabetic/diabetic PWH highlights differences in PBMCs by metabolic disease

(A) UMAP and corresponding heatmap of 1.5 million $CD45^+$ cells from the PBMCs of 38 participants depicting clusters of monocytes, CD4 T cells, CD8 T cells, B cells, monocytes, and NK cells.

(B) UMAPs stratified by metabolic disease highlighting differences using an overlay approach. Clusters higher in prediabetic/diabetic are in magenta and those higher in non-diabetic are in blue.

(C) Heat map shows all the markers that were used to define clusters in the UMAPs. The median fold difference bar (purple clusters are higher in prediabetics/diabetics and blue are higher in non-diabetic PWH). Clusters in the heat map are grouped according to the bigger clusters ($CD4^+$ T cells, $CD8^+$ T cells, Monocytes, B cells, NK cells, DN (double negative $CD3^+$ T cells), and immune complexes).

See Figure S1.

We employed the T-REX workflow as an unbiased, granular approach to visualize distinct cell populations that varied between non-diabetic and prediabetic/diabetic PWH and marker enrichment modeling (MEM) to identify the markers that define each of the different clusters.[22,23] The UMAP (**Figure 2A**) displays the distribution of cells from both non-diabetic (blue) and prediabetic/diabetic (red) PWH and the clusters that were greater than 95% different between the two groups (**Figure 2B**). We found $CD14^+$ clusters outside of the primary monocyte population, adjacent to the $CD4^+$ T cells, $CD8^+$ T cells, $CD19^+$ B cells, and NK cells (**Figure 2C**). Unexpected markers (FOXP3, CTLA4, and CRTH2) also defined the clusters with immune complexes, suggesting additional potential biomarkers for further investigation (**Figure 2D**). While FOXP3 and CTLA4 are constitutively expressed on $CD4^+$ T regulatory cells, they can be expressed on activated cells. We also compared the cluster sizes identified using T-REX between non-diabetic vs. prediabetic/diabetic using non-parametric analysis. All immune complex cluster sizes except cluster 3 ($CD19^+$ $CD14^+$ complex) remained significantly higher (**Figure 2E**). UMAPs highlighting the expression of CD14 and FOXP3 on all $CD45^+$ cells within the clusters with monocyte complexes, and not in other cells present in PBMCs are shown (**Figure 2F**). In summary, with TREX, the same clusters were different when we generated the UMAPs stratified by diabetes status in Figure 1b. The complexes were present within each

177 cluster of T cells/ B cells/ NK cells and Monocytes. We chose to focus on $CD3^+$ $CD14^+$ T -cell
178 monocyte complexes going forward, in the context of HIV reservoir and diabetes.
179
180 When we analyzed $CD3^+CD4^+$ T cells, we found several subclusters within $CD4^+$ T cells that
181 were also $CD14^+$ (**Figure S2A**). The $CD4^+$ T cell - $CD14^+$ monocyte clusters were mostly
182 present in people with prediabetes/diabetes (**Figure S2B-C**). The T-REX workflow generated a
183 similar result, with the three larger clusters that were higher with glucose intolerance also co-
184 expressed CTLA4, FOXP3, and CD14 (**Figure S2D**). Similarly, several $CD3^+CD8^+$ T cell
185 subclusters were $CD14^+$ (**Figure S3A**). Stratification by the metabolic group demonstrated that
186 the $CD8^+CD14^+$ subclusters were mainly present in the prediabetic/diabetic participants (**Figure**
187 **S3B**). This was confirmed using T-REX analysis, with two of the main clusters labeled
188 *preDM/DM1 and 2*, which included cells with CD14, CTLA4, and FOXP3 co-expression (**Figure**
189 **S3C-D**).

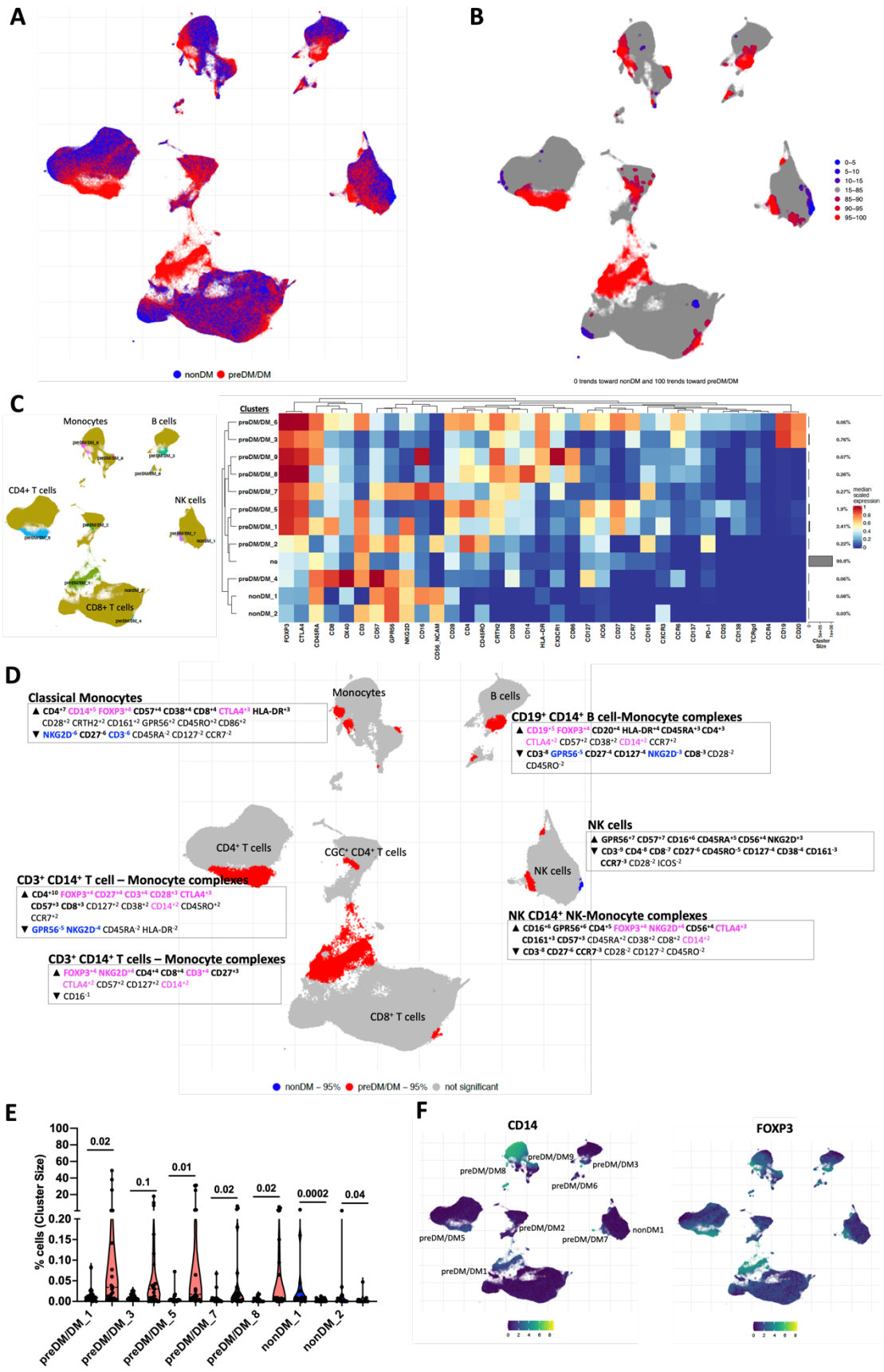
A
nonDM
preDM/DM
B
0–5
5–10
10–15
15–85
85–90
90–95
95–100
0 trends toward nonDM and 100 trends toward preDM/DM
C
Monocytes
B cells
CD4+ T cells
NK cells
CD8+ T cells
Clusters
preDM/DM_6
preDM/DM_3
preDM/DM_9
preDM/DM_8
preDM/DM_7
preDM/DM_5
preDM/DM_1
preDM/DM_2
na
preDM/DM_4
nonDM_1
nonDM_2
FOXP3
CTLA4
CD45RA
CD8
OX40
CD3
CD57
GPR56
NKG2D
CD16
CD56_NCAM
CD28
CD4
CD45RO
CRTH2
CD38
CD14
HLA-DR
CXCR1
CD86
CD127
ICOS
CD27
CCR7
CD161
CXCR3
CCR6
CD137
PD-1
CD25
CD138
TCRgd
CCR4
CD19
CD20
median scaled expression
Cluster Size
D
Classical Monocytes
▲ CD4+7 CD14+5 FOXP3+4 CD57+4 CD38+4 CD8+4 CTLA4+3 HLA-DR+3
CD28+2 CRTH2+2 CD161+2 GPR56+2 CD45RO+2 CD86+2
▼ NKG2D-6 CD27-6 CD3-6 CD45RA-2 CD127-2 CCR7-2
Monocytes
B cells
CD19+ CD14+ B cell-Monocyte complexes
▲ CD19+3 FOXP3+4 CD20+4 HLA-DR+4 CD45RA+3 CD4+3
CTLA4+2 CD57+2 CD38+2 CD14+2 CCR7+2
▼ CD3-8 GPR56-5 CD27-4 CD127-4 NKG2D-3 CD8-3 CD28-2
CD45RO-2
CD4+ T cells
CGC+ CD4+ T cells
NK cells
NK cells
▲ GPR56+7 CD57+7 CD16+6 CD45RA+5 CD56+4 NKG2D+3
▼ CD3-9 CD4-8 CD8-7 CD27-6 CD45RO-5 CD127-4 CD38-4 CD161-3
CCR7-3 CD28-2 ICOS-2
CD3+ CD14+ T cell – Monocyte complexes
▲ CD4+10 FOXP3+4 CD27+4 CD3+4 CD28+3 CTLA4+3
CD57+3 CD8+3 CD127+2 CD38+2 CD14+2 CD45RO+2
CCR7+2
▼ GPR56-5 NKG2D-4 CD45RA-2 HLA-DR-2
NK CD14+ NK-Monocyte complexes
▲ CD16+6 GPR56+6 CD4+5 FOXP3+4 NKG2D+4 CD56+4 CTLA4+3
CD161+3 CD57+3 CD45RA+2 CD38+2 CD8+2 CD14+2
▼ CD3-8 CD27-6 CCR7-3 CD28-2 CD127-2 CD45RO-2
CD3+ CD14+ T cells – Monocyte complexes
▲ FOXP3+4 NKG2D+4 CD4+4 CD8+4 CD3+4 CD27+3
CTLA4+2 CD57+2 CD127+2 CD14+2
▼ CD16-1
CD8+ T cells
nonDM – 95%
preDM/DM – 95%
not significant
E
% cells (Cluster Size)
0.02
0.1
0.01
0.02
0.02
0.0002
0.04
preDM/DM_1
preDM/DM_3
preDM/DM_5
preDM/DM_7
preDM/DM_8
nonDM_1
nonDM_2
F
CD14
preDM/DM9
preDM/DM8
preDM/DM3
preDM/DM6
preDM/DM5
preDM/DM2
preDM/DM7
nonDM1
preDM/DM1
FOXP3

190

Figure 2. Classical monocytes complex with T cells, NK cells, and B cells are increased in the peripheral blood of PWH with glucose intolerance.

(A) UMAP of $CD45^+$ cells from non-diabetic (blue), prediabetic/diabetic PWH (red).
(B) Clusters identified by the T-REX algorithm that are increased and decreased with prediabetes/diabetes (0 trends towards non-diabetic and 100 towards prediabetic/diabetic).
(C) Clusters higher with prediabetes/diabetes (preDM/DM) or without diabetes (NonDM) are shown along with the heat map that highlights markers that define the cells within the clusters.
(D) The enrichment scores of markers (increased and decreased) for selected clusters are shown over the UMAP, adjacent to the clusters. Among the markers that characterize the clusters, magenta (increased markers), and blue (decreased).
(E) Violin plots showing proportions of select subclusters that are significantly different between non-diabetes (non-DM and prediabetes/diabetes (preDM/DM).
(F) UMAPs show CD14 and FOXP3 expression on the clusters.

Statistical analysis by Mann-Whitney test (E). See Figures S2 and S3.

207 **$CD3^+$ T cell - $CD14^+$ monocyte complexes increase in longitudinal samples**

208 To confirm that the complexes identified by mass cytometry were monocytes complexed to
209 other immune cells and not artifacts, we stained PBMCs with a flow cytometry panel to identify
210 cells with $CD3^+$ and $CD14^+$ expression (**Figure 3A**). The Z channel shows CD3 expression on
211 lymphocytes and monocytes (**Figure 3A**). Based on the two-dimensional plots, $CD3^+CD14^+$ T
212 cell complexes are among the larger monocyte cells (larger and more granular). We then sorted
213 $CD14^+$ monocytes and $CD3^+$ $CD14^+$ T cell-monocyte complexes and used light microscopy to
214 image the cells. Compared to $CD14^+$ cells alone, the $CD3^+$ $CD14^+$ complexes had a higher
215 proportion of cells with presumed immunological synapses due to the proximity of cells and
216 flattening at the connecting points (**Figure 3B**).

217

218 We next analyzed longitudinal PBMC samples from 37 of the 38 participants who had a second
219 visit 2-3 years after the first, to assess whether the proportion of $CD3^+$ $CD14^+$ complexes
220 remained stable or varied over time. $CD3^+$ $CD14^+$ T cell-monocyte complexes ranged from
221 0.07% to 11.5% of $CD3^+$ T cells by flow cytometry at the first visit and 0.55% to 9.5% at the
222 second visit. We observed a significant increase ($p=0.03$) in the proportion of $CD3^+$ $CD14^+$ T cell
223 – monocyte complexes, as a proportion of $CD3^+$ live cells, from the first to second visit (**Figure**
224 **3C**). When stratified by diabetes status, there was a greater increase in $CD3^+$ $CD14^+$ T cell-
225 monocyte complexes among the non-diabetic compared to the prediabetic/diabetic PWH
226 (**Figure 3D**). This observation suggests that a higher proportion of circulating T cell–monocyte
227 complexes in prediabetes/diabetes represents more of a terminal state and that once PWH
228 have prediabetes or diabetes, then metabolic disease and related complications are frequent,
229 while some of the PWH without diabetes may still be progressing in this direction as they age.

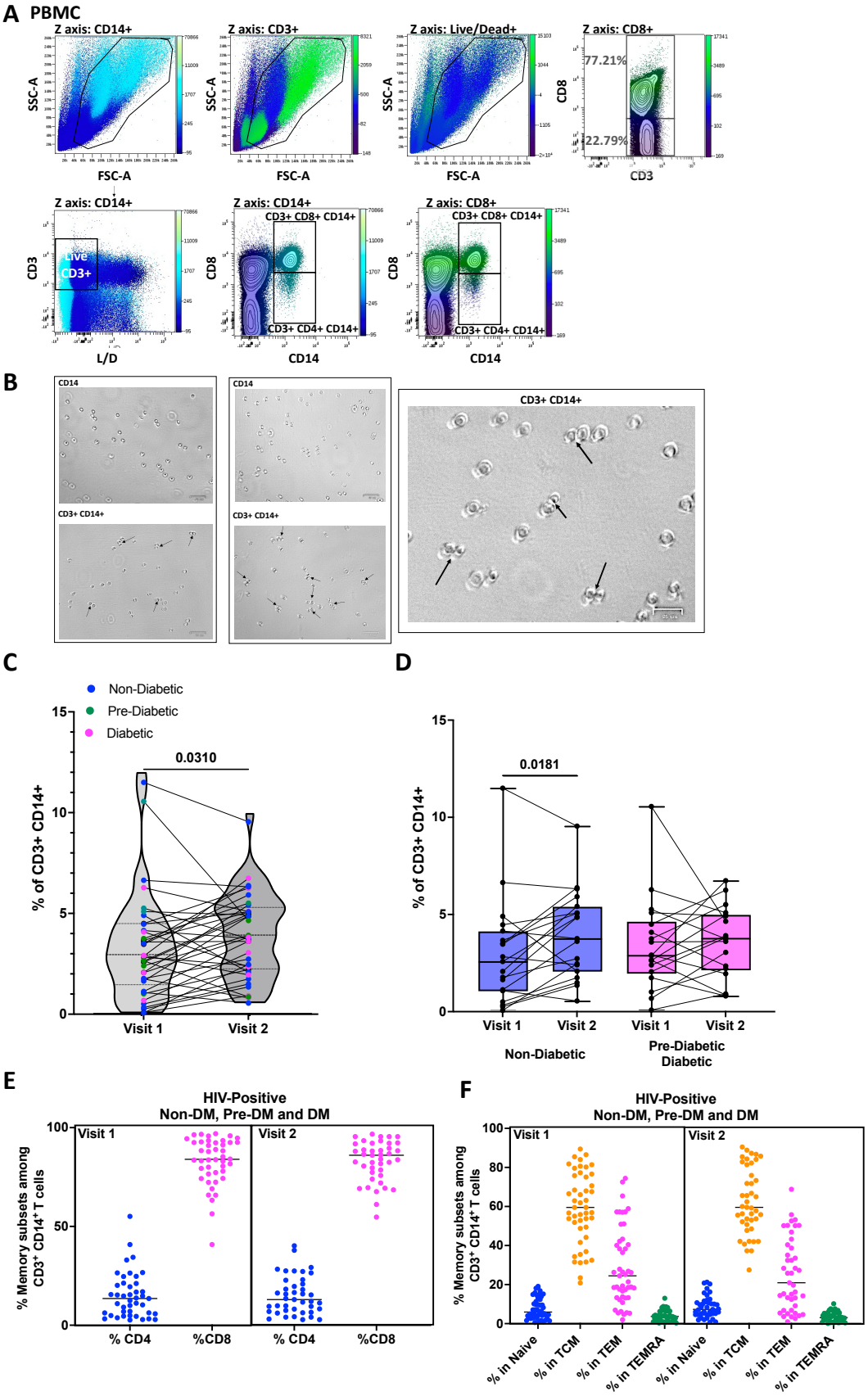
A PBMC
Z axis: CD14+
Z axis: CD3+
Z axis: Live/Dead+
Z axis: CD8+
SSC-A
FSC-A
CD8
CD3
77.21%
22.79%
Live
CD3+
L/D
CD3+ CD8+ CD14+
CD3+ CD4+ CD14+
CD14
B
CD14
CD3+ CD14+
C
Non-Diabetic
Pre-Diabetic
Diabetic
0.0310
% of CD3+ CD14+
Visit 1
Visit 2
D
0.0181
Non-Diabetic
Pre-Diabetic
Diabetic
E
HIV-Positive
Non-DM, Pre-DM and DM
% Memory subsets among CD3+ CD14+ T cells
% CD4
%CD8
F
% in Naive
% in TCM
% in TEM
% in TEMRA

230

Figure 3. $CD14^+$ classical monocytes form complexes primarily with $CD8^+$ and central memory T cells.
(A) Two-dimensional flow cytometry plot of PBMCs showing CD14, CD3, and Live/Dead stains on PBMCs. $CD3^+$ cells were gated on live cells (including lymphocytes and monocytes), followed by a two-dimensional plot of $CD8^+$ and $CD14^+$ cells.
(B) Bright-field images of $CD14^+$ and $CD3^+$ $CD14^+$ cells.
(C) Violin plot showing % $CD3^+$ $CD14^+$ T cell-monocyte complexes in longitudinal time points 2-3 years apart.
(D) Box plots plot showing % $CD3^+$ $CD14^+$ T cell-monocyte complexes in longitudinal time points stratified by diabetes status.
(E) Dot plot showing proportions of $CD4^+$ and $CD8^+$ T cells among CD3+ CD14+ complexes.
(F) Dot plot showing proportions of memory $CD3^+$ T cells (naïve, $CD45RO^-$ $CCR7^+$, TEM, $CD45RO^+$ $CCR7^-$, TCM, $CD45RO^+$ $CCR7^+$, TEMRA, $CD45RO^-$ $CCR7^-$)

Statistical analyses were performed using Mann Whitney U test (C) and Wilcoxon matched pair signed ranks test (D).

T cell-$CD14^+$ monocyte complexes are positively associated with fasting blood glucose and hemoglobin A1C

Based on the observed differences in $CD3^+$ $CD14^+$ complexes by diabetes status, we posited that the complexes may drive glucose intolerance. We used partial Spearman rank correlation analysis adjusted for age, sex, and BMI to assess whether the circulating immune complexes were associated with fasting blood glucose and hemoglobin A1C. We found that $CD8^+$ T cell – $CD14^+$ monocyte complexes were associated with fasting blood glucose ($p<0.05$) and hemoglobin A1C ($p<0.01$) (**Figure 4A**). The NK cell – $CD14^+$ monocyte cluster was also positively associated with fasting blood glucose ($p<0.05$) but not hemoglobin A1C. $CD4^+$ T cell – $CD14^+$ monocyte complexes were only positively associated with hemoglobin A1C ($p<0.01$) and not fasting blood glucose (**Figure 4A**).

Greater systemic inflammation, in aggregate, is associated with an increased risk of cardiovascular and metabolic disease[24]. There were no significant differences in plasma cytokines among the 38 participants by group comparison, including IL-1β, IFN-γ, TNF-α, IL-6, IL-17, and IL-10 (Data not shown). We performed Spearman rank correlation analyses adjusted for factors related to HIV (CD4:CD8 ratio, duration of antiretroviral therapy) and diabetes

265 (hemoglobin A1C). We found that the immune complexes with monocytes [Clusters18, 19, 26,
266 27, 28, and 29] were strongly correlated with each other. Notably, all clusters were negatively
267 correlated with circulating $CD4^+$ T regulatory cells (CL 25) (**Figure 4B**). $CD8^+$ T cells ($p<0.01$), B
268 cells ($p<0.05$), and NK cells ($p<0.05$) complexed with monocytes were also negatively
269 correlated with plasma IL-10 ($p<0.05$). The $CD4^+$ $CD14^+$ T cell-monocyte cluster was negatively
270 correlated with IL-10 but this was not statistically significant ($p=0.067$). Cluster 32 was
271 comprised of $CD3^+$ T cells (both CD4 and CD8) complexed with $CD14^+$ monocytes that were
272 less correlated with the other complexes. This was a much smaller cluster than all other
273 complexes and positively correlated with plasma sCD163 ($p=0.075$) and plasma IL-17A
274 ($p=0.03$). We considered whether the relationship between the immune complexes and IL-
275 10/CD4 T regulatory cells might depend on the level of blood glucose. To test this hypothesis,
276 we included an interaction term (hemoglobin A1C*IL-10 and hemoglobin A1C*CD4 T regulatory
277 cells) in a linear regression model with the immune complexes as the dependent variables
278 (**Figure S4A**). The coefficients for the interaction terms were negative and statistically
279 significant (**Figure S4B**), suggesting that the effect of IL-10 and $CD4^+$ T regulatory cells on the
280 immune complexes decreases as hemoglobin A1C increases or vice versa. In other words, the
281 relationship between the immune complexes and hemoglobin A1C is weaker for individuals with
282 higher levels of IL-10 or CD4 T regulatory cells.

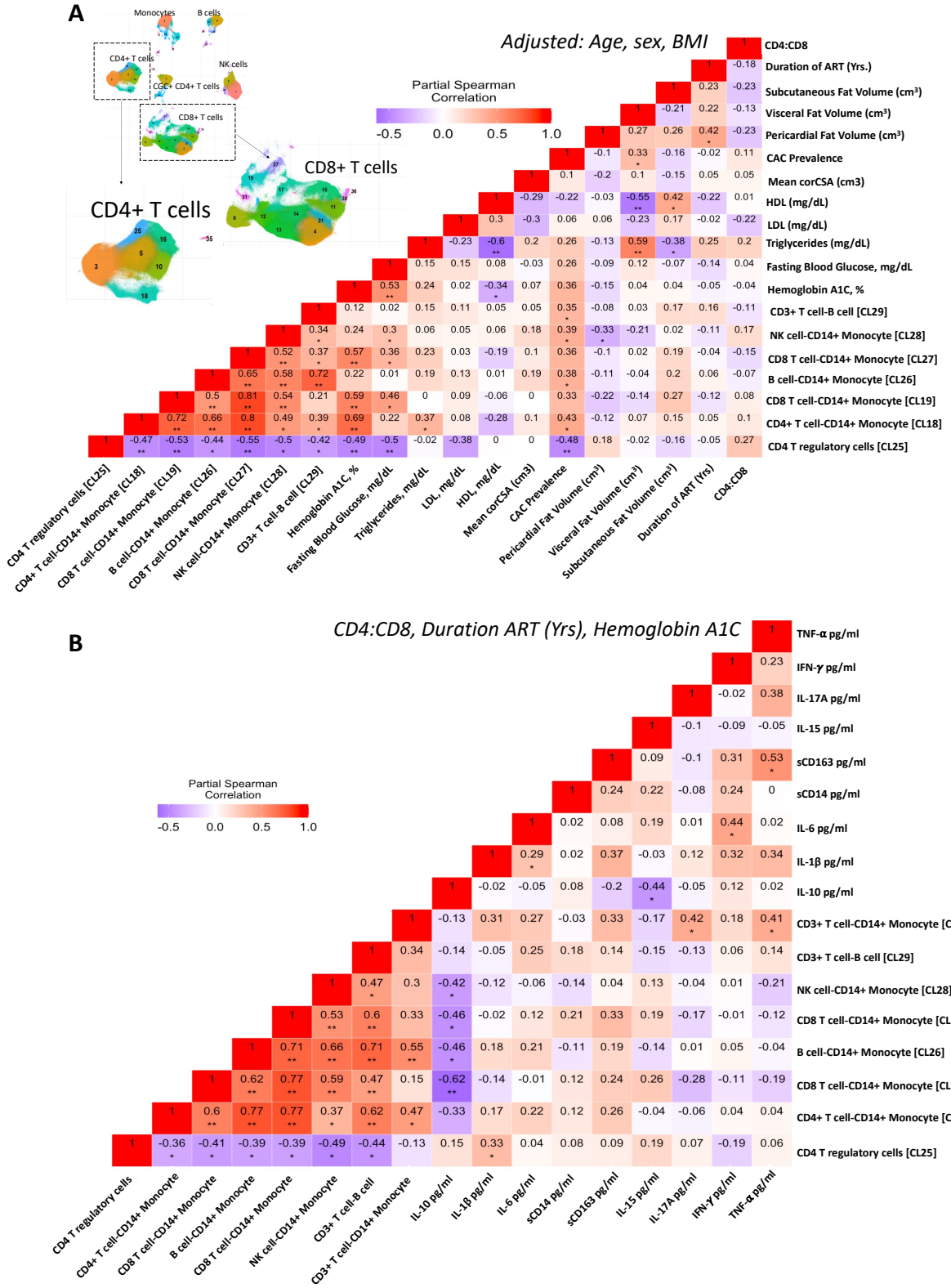
A
Monocytes
B cells
CD4+ T cells
NK cells
CGC+ CD4+ T cells
CD8+ T cells
CD8+ T cells
CD4+ T cells
Adjusted: Age, sex, BMI
Partial Spearman Correlation
-0.5 0.0 0.5 1.0
CD4:CD8
Duration of ART (Yrs.)
Subcutaneous Fat Volume (cm³)
Visceral Fat Volume (cm³)
Pericardial Fat Volume (cm³)
CAC Prevalence
Mean corCSA (cm3)
HDL (mg/dL)
LDL (mg/dL)
Triglycerides (mg/dL)
Fasting Blood Glucose, mg/dL
Hemoglobin A1C, %
CD3+ T cell-B cell [CL29]
NK cell-CD14+ Monocyte [CL28]
CD8 T cell-CD14+ Monocyte [CL27]
B cell-CD14+ Monocyte [CL26]
CD8 T cell-CD14+ Monocyte [CL19]
CD4+ T cell-CD14+ Monocyte [CL18]
CD4 T regulatory cells [CL25]
CD4 T regulatory cells [CL25]
CD4+ T cell-CD14+ Monocyte [CL18]
CD8 T cell-CD14+ Monocyte [CL19]
B cell-CD14+ Monocyte [CL26]
CD8 T cell-CD14+ Monocyte [CL27]
NK cell-CD14+ Monocyte [CL28]
CD3+ T cell-B cell [CL29]
Hemoglobin A1C, %
Fasting Blood Glucose, mg/dL
Triglycerides, mg/dL
LDL, mg/dL
HDL, mg/dL
Mean corCSA (cm3)
CAC Prevalence
Pericardial Fat Volume (cm³)
Visceral Fat Volume (cm³)
Subcutaneous Fat Volume (cm³)
Duration of ART (Yrs)
CD4:CD8
B
CD4:CD8, Duration ART (Yrs), Hemoglobin A1C
Partial Spearman Correlation
-0.5 0.0 0.5 1.0
TNF-α pg/ml
IFN-γ pg/ml
IL-17A pg/ml
IL-15 pg/ml
sCD163 pg/ml
sCD14 pg/ml
IL-6 pg/ml
IL-1β pg/ml
IL-10 pg/ml
CD3+ T cell-CD14+ Monocyte [CL32]
CD3+ T cell-B cell [CL29]
NK cell-CD14+ Monocyte [CL28]
CD8 T cell-CD14+ Monocyte [CL27]
B cell-CD14+ Monocyte [CL26]
CD8 T cell-CD14+ Monocyte [CL19]
CD4+ T cell-CD14+ Monocyte [CL18]
CD4 T regulatory cells [CL25]
CD4 T regulatory cells
CD4+ T cell-CD14+ Monocyte
CD8 T cell-CD14+ Monocyte
B cell-CD14+ Monocyte
CD8 T cell-CD14+ Monocyte
NK cell-CD14+ Monocyte
CD3+ T cell-B cell
CD3+ T cell-CD14+ Monocyte
IL-10 pg/ml
IL-1β pg/ml
IL-6 pg/ml
sCD14 pg/ml
sCD163 pg/ml
IL-15 pg/ml
IL-17A pg/ml
IFN-γ pg/ml
TNF-α pg/ml

283

284

285 **Figure 4. T cell-Monocyte immune complexes positively associated with blood glucose**
286 **are negatively associated with IL-10.**
287 (A) Heatmap shows partial Spearman correlation of immune complex clusters and CD4 T
288 regulatory cells and hemoglobin A1c, fasting blood glucose adjusted for age, sex, and BMI.
289 UMAP with clusters is included for reference.
290 (B) Heatmap shows partial Spearman correlation of immune complex clusters and CD4 T
291 regulatory cells and inflammatory cytokines (IL-10, IL-6, sCD14, sCD163, IL-15, IL-17, and IL-
292 1β] adjusted for CD4:CD8, antiretroviral therapy duration, and hemoglobin A1C.
293
294 See Figure S4.
295

296 **CD4$^+$ T cells complexed with CD14$^+$ monocytes include TH1, TH17, and TH2 phenotypes**

297 To better characterize the CD4$^+$ T cells complexed with CD14$^+$ monocytes, we first analyzed the
298 memory subsets using CCR7 and CD45RO (**Figure 5A**). Similar to our analysis with total CD3$^+$
299 T cells, CD14$^+$ monocytes were largely complexed with CD4$^+$ TCM and TEM cells in both non-
300 diabetic and prediabetic/diabetic PWH (**Figure 5B**). Several markers of activation were used to
301 define activated CD4$^+$ T cells (CD137/OX40 and HLADR/CD38). Representative two-
302 dimensional flow charts show the expression of these markers on CD4$^+$ T cells from non-
303 diabetic and prediabetic/diabetic PWH (**Figure 5C**). In general, there was a significantly higher
304 proportion of activated, CD137$^+$ OX40$^+$ CD4$^+$ T cells and HLA-DR$^+$ CD38$^+$ CD4$^+$ T cells in
305 prediabetic/diabetic PWH compared to non-diabetic (**Figure 5D, left panels**). Focusing on
306 immune complexes, we observed that CD4$^+$ CD14$^+$ T cells had a higher proportion of CD137
307 and OX40 expressing cells (**Figure 5D, top right panel**). Irrespective of metabolic status, all
308 cells within immune complexes were HLADR$^+$ CD38$^+$. Circulating activated T cells and immune
309 complexes were correlated with fasting blood glucose (**Figure 5F**). Using chemokine receptor
310 markers, we defined CD4$^+$ T helper subsets within the T cell-monocyte complexes. CD4$^+$ T cells
311 from prediabetic/diabetic PWH compared to non-diabetic had a significantly higher proportion of
312 TH2, TH17, and TH1 CD4$^+$ T cells (**Figure 5G**). A similar trend was observed with CD4$^+$ CD14$^+$
313 T cell-monocyte complexes which had higher proportions of Th1 and Th17 cells. In summary,
314 the T-cell monocyte immune complexes consist of activated immune cells, enriched for
315 inflammatory memory subsets.

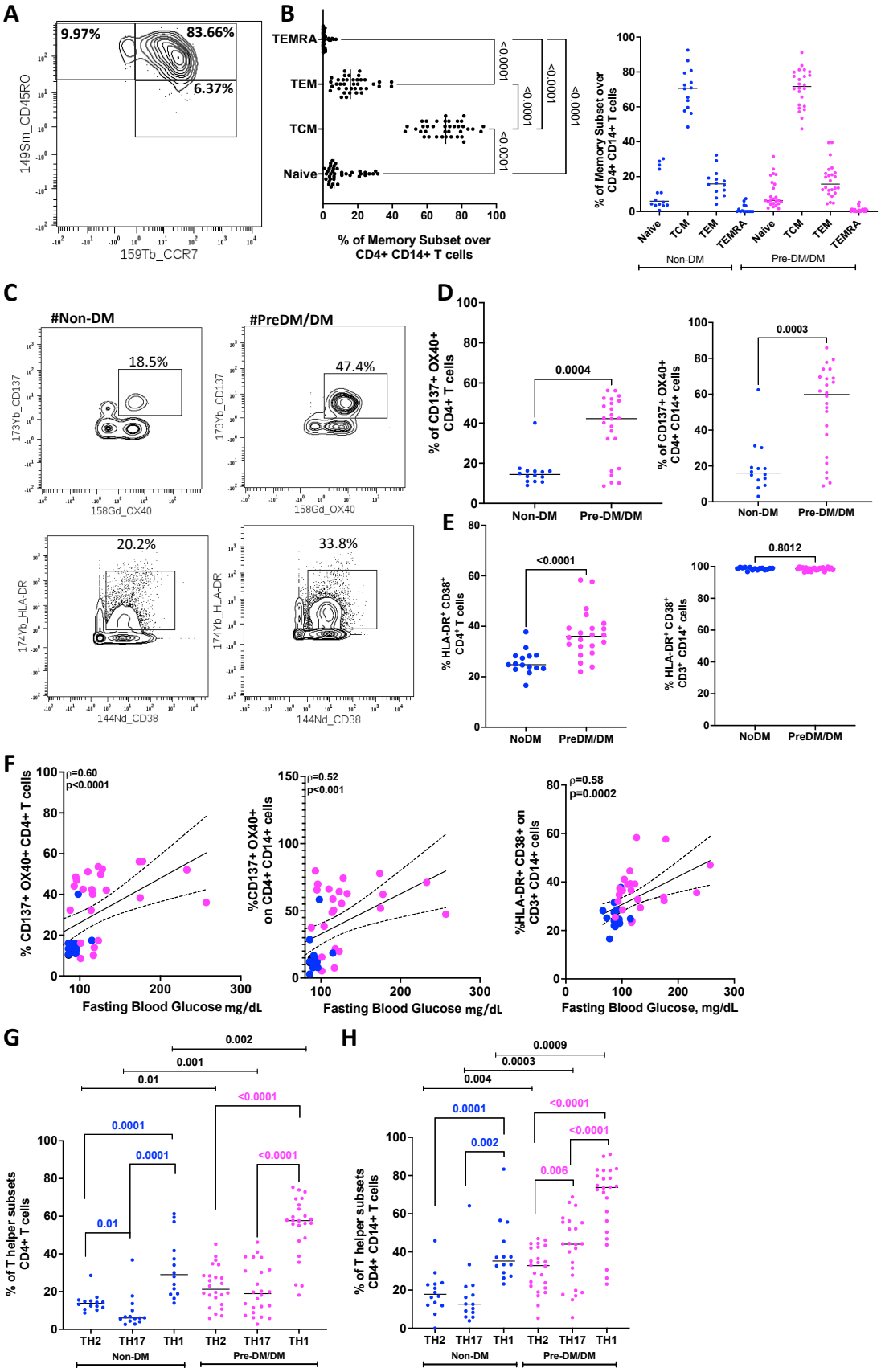
A
9.97%
83.66%
6.37%
149Sm_CD45RO
159Tb_CCR7
B
TEMRA
TEM
TCM
Naive
<0.0001
% of Memory Subset over CD4+ CD14+ T cells
% of Memory Subset over CD4+ CD14+ T cells
Naive
TCM
TEM
TEMRA
Non-DM
Pre-DM/DM
C
#Non-DM
#PreDM/DM
18.5%
47.4%
173Yb_CD137
158Gd_OX40
20.2%
33.8%
174Yb_HLA-DR
144Nd_CD38
D
% of CD137+ OX40+ CD4+ T cells
0.0004
% of CD137+ OX40+ CD4+ CD14+ cells
0.0003
Non-DM
Pre-DM/DM
E
% HLA-DR+ CD38+ CD4+ T cells
<0.0001
% HLA-DR+ CD38+ CD3+ CD14+ cells
0.8012
NoDM
PreDM/DM
F
% CD137+ OX40+ CD4+ T cells
ρ=0.60
p<0.0001
%CD137+ OX40+ on CD4+ CD14+ cells
ρ=0.52
p<0.001
%HLA-DR+ CD38+ on CD3+ CD14+ cells
ρ=0.58
p=0.0002
Fasting Blood Glucose mg/dL
G
% of T helper subsets CD4+ T cells
0.002
0.001
0.01
<0.0001
0.0001
0.0001
0.01
<0.0001
TH2
TH17
TH1
Non-DM
Pre-DM/DM
H
% of T helper subsets CD4+ CD14+ T cells
0.0009
0.0003
0.004
0.0001
<0.0001
0.002
<0.0001
0.006

316

Figure 5. $CD4^+$ T cells complexed with $CD14^+$ monocytes in prediabetic/diabetic PWH are activated with a larger proportion of TH17 and TH1 cells.
(A) Two-dimensional flow cytometry plots show memory $CD4^+$ T cells (Naïve, $CD45RO^-$ $CCR7^+$; TCM, $CD45RO^+$ $CCR7^+$; TEM $CD45RO^+$ $CCR7^-$; TEMRA $CD45RO^-$ $CCR7^-$).
(B) Memory $CD4^+$ T cell subsets in non-diabetic and prediabetic/diabetic PWH have a similar distribution of memory T cell subsets.
(C) Representative plots showing CD137/OX40 and HLA-DR/CD38 co-expression on CD4+ T cell – CD14+ monocyte complexes stratified by diabetes.
(D) Dot plots show % $CD137^+$ $OX40^+$ $CD4^+$ T cells and % $CD137^+$ $OX40^+$ $CD14^+$ complexes.
(E) Dot plots show % $HLA\text{-}DR^+$ $CD38^+$ $CD4^+$ T cells and % $HLA\text{-}DR^+$ $CD38^+$ $CD14^+$ complexes.
(F) Activated T cells -monocyte immune complexes are correlated with fasting blood glucose.
(G) PWH with pre-diabetes/diabetes have a higher proportion of TH2 (CRTH2/CCR4), TH17 (CCR6/CD161), and TH1 (CXCR3) cells stratified by diabetes.
(H) $CD4^+$ T helper cells within $CD4^+$ $CD14^+$ T cell-monocyte complexes have higher proportions of TH2, TH17, and TH1 cells.
Statistical analyses were performed using the Mann-Whitney U test (D-E), Spearman correlation (F), and the Kruskal-Wallis test (G-H).

T cell-monocyte pairs form stable complexes and have particles consistent with HIV

In order to understand the durability of the T cell-monocyte complexes given their abundance, we sorted $CD3^+$ T cell-$CD14^+$ monocyte immune complexes and imaged them over 4.5 hours. Time-lapse imaging of the $CD3^+$ $CD14^+$ T cell-monocyte immune complexes shows dynamic and heterogeneous relationships between $CD14^+$ monocytes and $CD3^+$ T cells (**Figure 6A-B, movies CD and E**). We observed several stable complexes over a period of 5 hours (**Figure 6C, D**) and a proportion of monocytes (antigen-presenting cells, APCs) that transiently interacted with T cells (**Figure 6E**).

Macrophages are HIV reservoirs that may effectively form synapses and infect $CD4^+$ T cells. [25] We hypothesized that HIV transfer may be enhanced by T cell-monocyte complexes in circulation. We sorted $CD3^+$ $CD14^+$ T cell-monocyte complexes and employed transmission electron microscopy (TEM) to capture the T cell and monocyte pairs interacting with high resolution. We observed T cells in immunological synapses with monocytes (**Figure 6F-i,ii**) with 100nm particles in T cells-monocyte pairs (**Figure 6F-i,ii**) and T cells among sorted $CD3^+$ $CD14^+$ T cell-monocyte complexes consistent with HIV (**Figure 6G**).

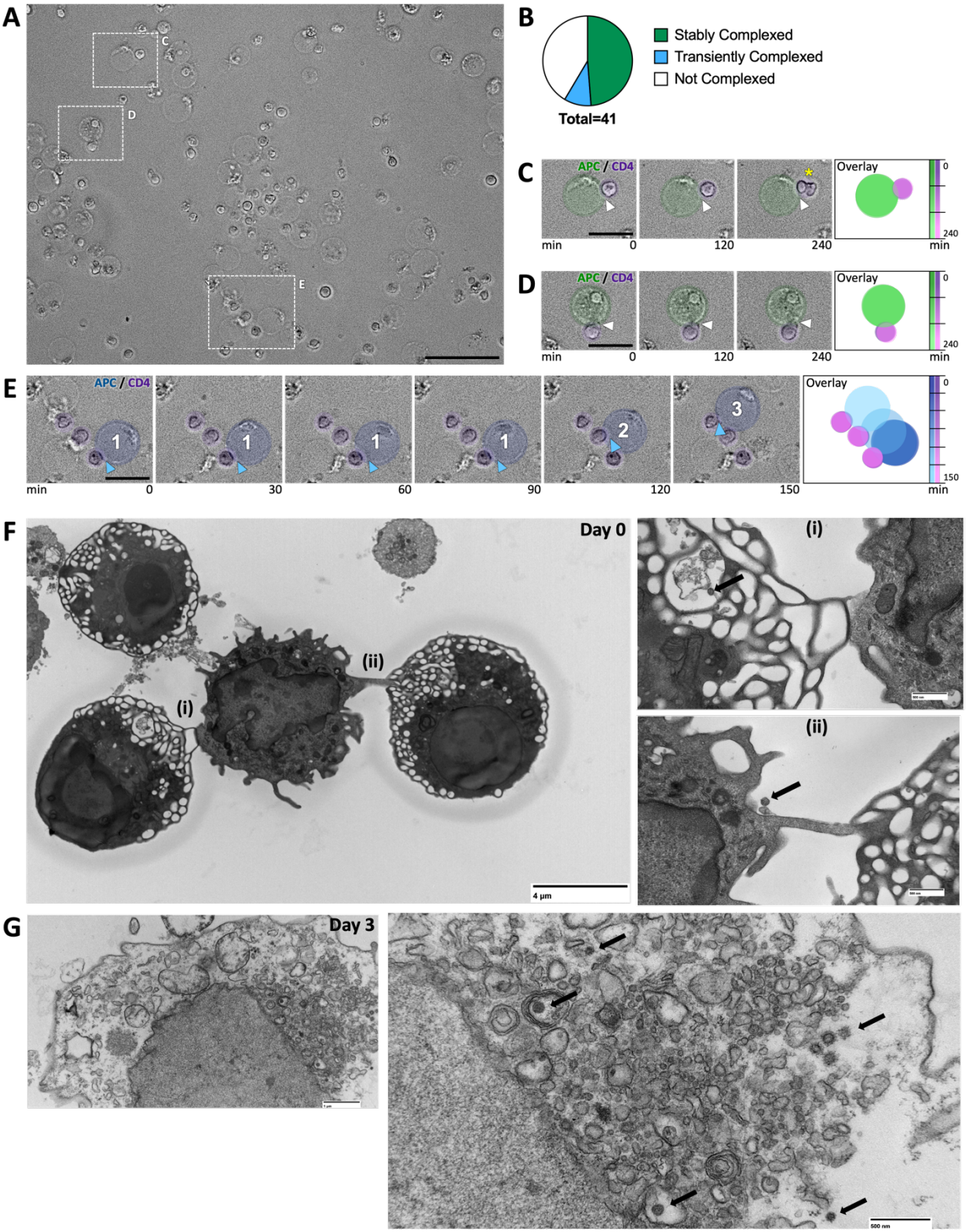

Figure 6. CD3⁺ CD14⁺ T cell - monocytes form stable complexes
(A) Phase-contrast microscopy of sorted CD3⁺ CD14⁺ T cell-monocyte complexes at time 0.

355 (B) Pie chart showing the percentage of (CD14 antigen presenting cells (APCs) that are stably
356 associated with T cells, transiently associated with T cells or not associated with T cells over
357 4.5hrs.
358 (C & D) Show insets of stable complexes, right hand panel shows the time overlay and the color
359 code. A yellow asterisk (*) in c marks a T cell that proliferates. Scale bars – purple pseudocolor
360 defines T cell and green marks APC.
361 (E) Time series demonstrating transient interactions between APC and three T cells (marked
362 1,2,3). Blue arrowheads and numbers mark point of interactions between APC and T cells.
363 (F) TEM of $CD3^+$ $CD14^+$ T cell-monocyte complexes. Inset highlights ultrastructural cell-cell
364 interactions (i) and (ii) and the presence of 100nm diameter particles (black arrow).
365 (G) TEM of $CD3^+$ T cell among sorted $CD3^+$ $CD14^+$ T cell-monocyte complexes 3 days post-
366 culture. Enlarged image (i) highlighting 100nm diameter particles (black arrow).
367 *Scale bars are 50μm A, 20μm C-E, 4μM F, 500nm F(i), F(ii), G (i), and 1μm G.*
368 See movies CD and E.

369 Using ddPCR, we quantified HIV DNA in sorted $CD4^+$ T cells, $CD14^+$ monocytes, and $CD3^+$
370 $CD14^+$ T cell-monocyte complexes from 6 PWH on antiretroviral therapy. Representative
371 images show LTR (blue) and RNAse P copies (green) in $CD3^+$ $CD14^+$ complexes (**Figure 7A**),
372 $CD4^+$ T cells (**Figure 7B**), and $CD14^+$ cells (**Figure 7C**). We found that $CD3^+$ $CD14^+$ T cell-
373 monocyte complexes had significantly more HIV DNA copies per million cells compared to
374 paired single $CD4^+$ T cells and $CD14^+$ monocytes (**Figure 7D-E**). Monocytes are reported to be
375 infected with latent human CMV, therefore used ddPCR to quantify CMV. [26] We did not detect
376 CMV DNA using three different sets of primers against US28, gB, and IE-1 (**data not shown**) in
377 immune complexes from all 6 participants (ages 24 to 59). Taken together, we were able to
378 detect HIV using ddPCR, which was highest in $CD3^+$ $CD14^+$ T cell-monocyte complexes.
379

380 If the immunological synapses between $CD3^+$ T cells and $CD14^+$ monocytes are an antigen-
381 driven process, we posited that clonally expanded T cells could be present within the $CD3^+$
382 $CD14^+$ complexes. Among 4 representative participants with higher HIV DNA copies in their
383 $CD3^+$ T cell-$CD14^+$ monocyte complexes, we index-sorted single complexes per well and
384 sequenced the $\alpha\beta$ TCR chains. The majority of the TCRs were single clones with a few clonal
385 TCRs (>2 T cells with identical CDR3), (**Figure 7F**). We used TCRmatch
386 (http://tools.iedb.org/tcrmatch/) to predict the antigen specificity of the clonal TCRs among those

387 identified. The majority of the clonal (CDR3 >2) TCRs that we found in public databases were
388 predicted to bind viral antigens (CMV, EBV, SARSCoV2), with one predicted to bind HIV
389 [CASKEGGAGGYTF] (**Table S3**). In addition, two CDR3 were predicted to bind an epitope from
390 the coagulation factor VIII. In summary, these data suggest that circulating T cell-monocyte
391 complexes may be partly driven by the presentation of herpes viral antigens. In PWH,
392 monocytes may be complexed with HIV-infected T cells, which places the monocyte in proximity
393 to infected cells to allow the formation of functional synapses.
394
395 **T cell-monocyte complexes have RNA transcriptomes enriched for genes important for**
396 **activation and adhesion**
397 We performed a single-cell transcriptomic analysis of PBMCs from a participant with a large
398 proportion of T cell-monocyte complexes as determined by CyTOF and flow cytometry. Using
399 CITE seq and RNA transcriptomic profiles, we classified immune cell complexes/doublets that
400 would have been excluded from further analysis based on traditional analysis approaches.
401 UMAP shows the different cell types that were classified based on their transcriptomic profile
402 (**Figure 7G**). We found several clusters that had immune complexes including a T cell-non-
403 classical monocyte cluster, T cell-classical monocyte cluster, B cell-monocyte cluster, T cell-B
404 cell cluster, and megakaryocyte-T cell cluster**.** UMAPs and violin plots show CITE-seq
405 expression of several surface markers, CD14, CD16, CD3, CD4, CD69, and CD8 (**Figure 7H-I**).
406 Classical monocytes paired with T cells had an almost equal representation of T cells with
407 clonal and non-clonal TCRs. Non-classical monocytes on the other hand were mostly paired
408 with clonal TCRs (**Figure 7J**).
409

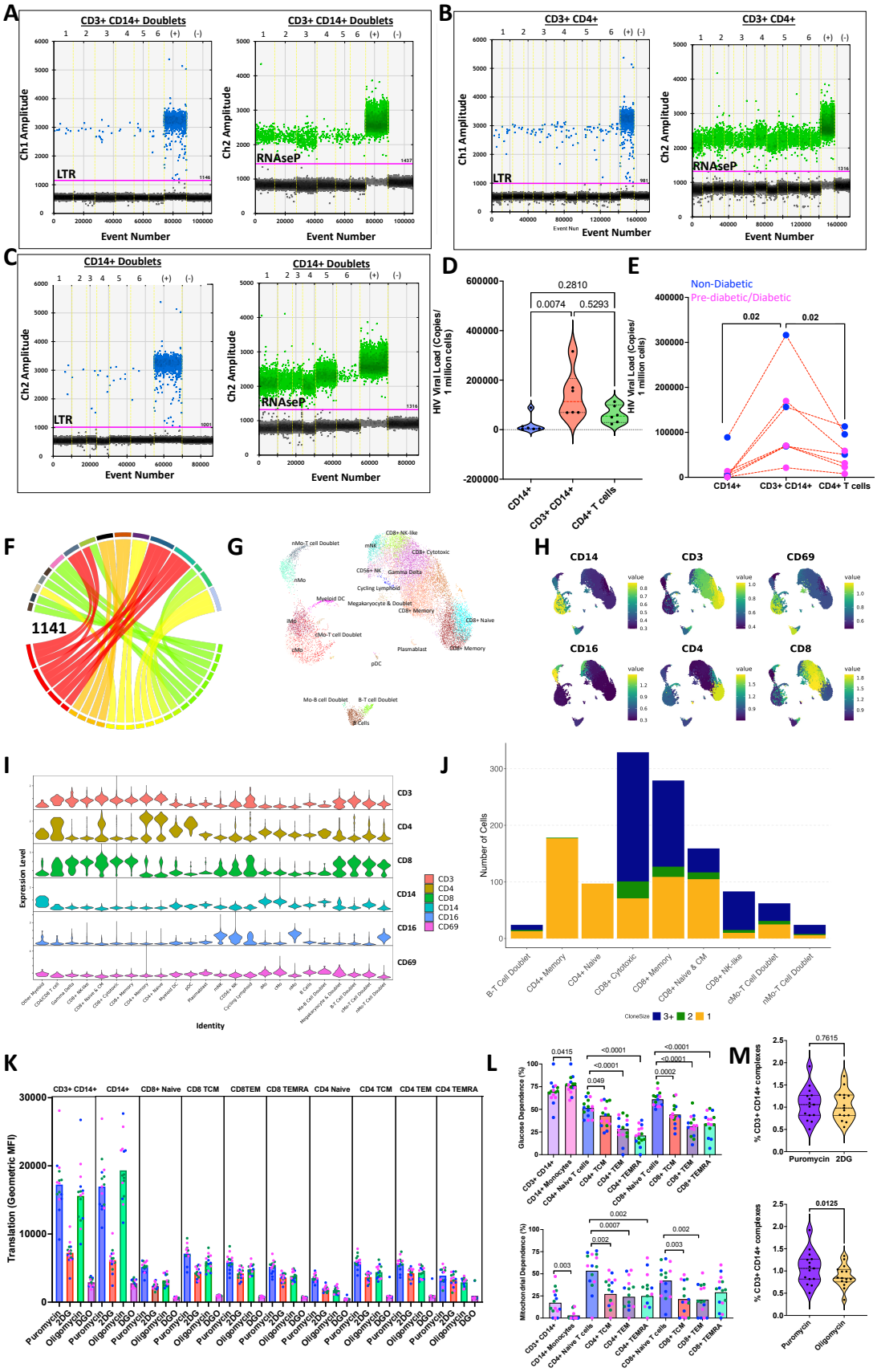
A
CD3+ CD14+ Doublets
Ch1 Amplitude
Ch2 Amplitude
LTR
RNAseP
Event Number
B
CD3+ CD4+
C
CD14+ Doublets
D
HIV Viral Load (Copies/ 1 million cells)
0.2810
0.0074
0.5293
CD14+
CD3+ CD14+
CD4+ T cells
E
Non-Diabetic
Pre-diabetic/Diabetic
0.02
0.02
F
1141
G
H
CD14
CD3
CD69
CD16
CD4
CD8
I
Expression Level
Identity
J
Number of Cells
CloneSize
K
CD3+ CD14+
CD14+
CD8+ Naive
CD8 TCM
CD8TEM
CD8 TEMRA
CD4 Naive
CD4 TCM
CD4 TEM
CD4 TEMRA
Translation (Geometric MFI)
L
Glucose Dependence (%)
Mitochondrial Dependence (%)
M
% CD3+ CD14+ complexes
0.7615
Puromycin
2DG
0.0125
Oligomycin

410

411 **Figure 7. $CD3^+$ $CD14^+$ T cell-monocyte complexes have more copies of HIV compared to**
412 **$CD4^+$ T cells and $CD14^+$ monocytes alone and are transcriptionally more activated**
413 **through direct antigen presentation.**
414 (A) Representative ddPCR plot showing HIV (blue) and RNase P (green) copies in sorted $CD3^+$
415 $CD14^+$ T cell-monocyte complexes.
416 (B) Representative ddPCR plot showing HIV (blue) and RNase P (green) copies in sorted $CD3^+$
417 $CD4^+$ T cells.
418 (C) Representative ddPCR plot showing HIV (blue) and RNase P (green) copies in sorted
419 $CD14^+$ monocytes.
420 (D) Violin plot shows HIV viral copies per million cells from the 6 participants in each of the
421 sorted cell types – $CD14^+$, $CD3^+$ $CD4^+$, $CD3^+$ $CD14^+$.
422 (E) The line plot shows HIV viral copies in paired samples.
423 (F) Circos plot shows paired TCRαβ CDR3 sequences expressed on T cells complexed with
424 monocytes from one representative participant
425 (G) UMAP of PBMCs processed for 10X sequencing from a participant with a high proportion of
426 immune complexes, highlighting T cell-monocyte doublets, B cell-T cell doublets, and B cell-
427 monocyte doublets.
428 (H) UMAPs highlight surface marker expression on PBMCs using CITE seq barcoded
429 antibodies.
430 (I) Violin plots show the difference in the surface marker expression levels between all the cells.
431 (J) TCR sequences were obtained, and the stacked bar chart shows the total number of cells
432 with TCRs and is color-coded based on the clonality of the cells, with 2 or greater considered
433 clonal.
434 (K) Bar plots depict protein translation by measuring puromycin uptake (puromycin), and
435 changes in uptake with the addition of inhibitors (2DG, oligomycin, and 2DG plus
436 oligomycin(DGO)) for each subset of cells [$CD3^+$ $CD14^+$, $CD14^+$ monocytes, $CD16^+$ monocytes,
437 and CD4/CD8 T cell subsets (naïve, TCM, TEM and TEMRA) for 15 individuals (Blue: NonDM,
438 Green: PreDM and Magenta: DM).
439 (L) Bar plots show percent glucose dependence (top) and percent mitochondrial dependence
440 (bottom).
441 (M) The proportion of $CD3^+$ $CD14^+$ T cell-monocyte complexes decreases with the inhibition of
442 oxidative phosphorylation by oligomycin. There is no change in glucose inhibition by 2DG.
443 Statistical analysis using Kruskal Wallis (D), Wilcoxon test (E), Mann Whitney Test (L, M)
444 See Figure S5, S6 and S7 and Tables S5-S7

445 Differential gene expression of $CD3^+$ $CD14^+$ doublet cluster versus classical monocytes

446 (singlets) showed increased expression of genes that enrich for T cell activation [*CCL5, IL7R*,

447 *CD3E*, *CD2*, *CD8B*, *LCK, CD7, and* HLA-DPA1] and the adaptive immune response [*CD3E,*

448 *PRF1, GZMM, LIME1, SKAP1, and CD247]* (**Figure S5A, Table S4**). Genes involved in lipid

449 localization [*THBS1, RETN, ACSL1, TSPO, CD36, IRS2*], granulocyte activation, and

450 neutrophil-mediated immunity [*S100A12, S100A8, S100A9, CDA, MNDA, RETN, CD36,*

451 *GLUT3, LYZ*] were significantly higher in monocytes than in the T cell-monocyte complexes. On

452 the other hand, differential gene expression of $CD3^+$ $CD14^+$ T cell-monocyte complexes versus

453 T cells enriched for genes involved in antigen processing and presentation *[HLA-DRA, CD74,*
454 *HLA-DRB1, HLA-DQA1, HLA-DQB1, HLA-DPA1, HLA-DPB1*, and *HLA-DRB5*] (**Figure S7B,**
455 **Table S5**). Non-classical monocytes complexed with T cells were also transcriptionally different
456 compared to singlet non-classical monocytes. Similar to the classical monocytes, the T cell-
457 non-classical monocyte complexes enriched for genes involved in the adaptive immune
458 response [*CD3E, IL7R, CD8B, PRF1, GZMM, CD247, SKAP1, LIME1,* CD7, and *TNFAIP3* –
459 *bold genes were also upregulated in T cell-classical monocytes versus monocytes*]. Several
460 overlapping pathways were overrepresented in $CD16^+$ single-cell non-classical monocytes over
461 the T cell-non-classical monocyte complexes including neutrophil-mediated immunity
462 [*SERPINA1, FCER1G, FTH1, LGALS3, CD68, ATP6V0C, PSAP, CFD, STXBP2, SLC11A1,*
463 *S100A11, CMTM6*], granulocyte activation and platelet degradation [*TIMP1, SERPINA1,*
464 *FCER1G, PSAP, CFD, ALDOA, STXBP2, LYN,* and *PECAM1*] (**Figure S5C, Table S6**). The
465 differential gene expression between $CD3^+$ $CD16^+$ T cell-monocyte complexes versus T cells
466 had an over-representation of genes that enriched for several pathways including IL-10
467 production [*FCER1G, LILRA5, LILRB1, VSIR, PYCARD*, and *LGALS9*] and negative regulation
468 of T cell activation [*LST1, LYN, HMOX1, LGALS3, CD74, MNDA, LILRB1, VSIR, PTPN6, CD86,*
469 *CEBPB,* and *LGALS9*]. Pathways highly represented in T cells compared to these $CD3^+$ $CD16^+$
470 T cell-monocyte doublets included protein localization to the membrane (**Figure S5d Table S6**).
471
472 Our analysis of immune complexes from 10x sequencing data is confounded by complexes that
473 may be formed due to technical artifacts, where more than one cell ends in a single droplet.
474 Therefore, we used existing 10X sequencing data from sequenced PBMCs from individuals
475 receiving cardiac surgery (n=10), to create artificial clusters by combining single T cells and
476 monocytes. The differential gene expression between T cells-classical monocytes complexes
477 compared to artificial doublets (single memory T cells and classical monocytes grouped for
478 comparison) showed higher levels of *GNLY, HLA-DRA, HLA-DPA1, HLA-DPB1, HLA-DRB1,*

479 *MT-ND4, and MT-ND3* with overrepresentation of several pathways including MHCII antigen
480 presentation and TCR signaling (**Figure S6A-C, Table S6**). Taken together, these data suggest
481 that in vivo, monocytes form durable complexes with a subset of clonal memory T cells that
482 persist ex-vivo. The T cell-classical monocyte complexes have transcriptomes that suggest an
483 activated inflammatory response which differs from the artificial doublets.
484
485 Changes in metabolism can be very informative of the inflammatory state and functional profile
486 of immune cells. [27] While immune cells can rely on both glucose and mitochondria for energy
487 production, activated cells mostly rely on glycolysis. [28] We measured glucose and mitochondrial
488 dependencies of PBMCs *ex vivo* using SCENITH. Based on the puromycin uptake, $CD3^+$ $CD14^+$
489 T cell-monocyte complexes and $CD14^+$ monocytes at baseline appear to be more metabolically
490 active than T cells (**Figure 7K**). While both $CD14^+$ monocytes and $CD3^+$ $CD14^+$ immunologic
491 complexes were mainly glucose-dependent, the latter had a higher mitochondrial dependence
492 (**Figure 7L**). We next posited that if the immune synapse formation/maintenance is a high
493 energy function based on the presence of mitochondria close to the synapse (**Figure S7A-B**),
494 then incubation of PBMCs with metabolic pathway inhibitors (2DG, oligomycin) would affect the
495 proportions of immune complexes detectable by flow cytometry. While the proportion of $CD3^+$
496 $CD14^+$ complexes remained the same after inhibition of glycolysis with 2DG, there was a
497 significant decrease in the percent of detectable $CD3^+$ $CD14^+$ immune complexes with inhibition
498 of oxidative phosphorylation (**Figure 7M**). Taken together, these initial studies suggest that the
499 cells that make up the $CD3^+$ $CD14^+$ immune complexes may use both glycolysis and oxidative
500 phosphorylation, though inhibition of mitochondrial ATP synthesis reduced the proportion of
501 complexes.
502

503 **Discussion**

504 This study reveals that circulating immunologic monocytes complexed with T cells are increased
505 in the presence of glucose intolerance in PWH, suggesting that these immune cell interactions
506 may contribute to the elevated burden of diabetes and metabolic disease associated with long-
507 term HIV infection. Importantly, the immune complexes have RNA transcriptomes that
508 demonstrate an inflammatory profile. Additionally, there is an inverse association between the
509 immune complexes and anti-inflammatory responses like IL-10 and $CD4^+$ T regulatory T cells.
510 Many of these complexes remain intact over a 4-hour time-lapse ex-vivo, which suggests that
511 they form prolonged synapses that may be an additional driver of inflammatory response.
512 Although immune complexes in blood have traditionally been ignored, recent findings implicate
513 them in immune perturbation, [13] Among the possible explanations for the accumulation of
514 circulating immune complexes, are the presence of HIV within these complexes and the fact
515 that they are increased with glucose intolerance, maybe a reflection of a bidirectional and self-
516 reinforcing loop that exists between complex-driven inflammation (driven by HIV) and elevated
517 blood sugar.

518

519 Monocytes are important leukocytes that constitutively leave the circulation to survey tissue.
520 $CD14^+$ classical monocytes represent close to 90% of total monocytes and are more likely to
521 become macrophages after transmigration into tissues. On the other hand, $CD14^{lo}$ $CD16^+$ non-
522 classical monocytes tend to differentiate into dendritic cells and may re-enter the blood
523 circulation. [29] In PWH on antiretroviral therapy, replicating and integrated HIV can be detected
524 in circulating monocytes. [30-33] Although $CD14^{lo}$ $CD16^+$ non-classical monocytes may be more
525 prone to HIV infection, [34] due to the study design using CD3 and CD14 to detect the immune
526 complexes, we show here that HIV viral particles within $CD14^+$ cell-classical monocyte
527 complexes. Our imaging studies allow us to speculate that HIV could be transferred from either
528 cell type. Within tissues, macrophages infected with HIV can effectively transmit HIV to $CD4^+$ T

529 cells, suggesting these cellular interactions may be an important contributor to T cell loss and
530 the establishment of the cellular reservoir. [25,35,36]
531
532 HIV cure will require the elimination of viral reservoirs, which has been a challenge due to the
533 inability of the immune system to eliminate latently infected cells. [18,37] The field recognizes that
534 there is a lot of heterogeneity in the viral reservoir which includes both cell types as well as their
535 viral activation states including the latent virus that is not transcriptional active and the
536 transcriptionally active virus which can be in a spectrum plus or minus viral protein expression.
537 [37] The immune-complex imaging suggests that these complexes are heterogeneous, many of
538 which remain intact over a 5-hour window. Thus, these complexes may adhere to inflamed
539 endothelium and be recruited together and help establish and replenish viral reservoirs within
540 tissues. Future studies will investigate the recruitment of these cells to better understand this.
541 Interestingly, our T cell receptor sequencing data consisted of clonal cells however there were
542 no dominant clones to suggest that these complexes are driven by a single antigen. However,
543 based on previously published public TCRs which are limited by what has been studied, a large
544 proportion of the TCRs expressed were against EBC, CMV, HIV, and SARS-CoV2. While this
545 may be biased by predominant TCRs in public databases, it implies that other chronic infections
546 such as EBV and CMV may also be important. While we were able to detect HIV by droplet
547 digital PCR, we did not detect CMV DNA within these complexes. However, additional studies
548 that use multiple modalities for detecting viruses (HIV, CMV, EBV, Influenza antigens, DNA,
549 RNA transcripts) are warranted.
550
551 Chronic systemic inflammatory responses in PWH may partly explain the high incidence and
552 prevalence of diabetes. [38,39] Similarly, there is growing evidence inflammation is important in the
553 pathogenesis of type 2 diabetes. [40] IL-10 is an anti-inflammatory cytokine that is expressed by
554 several cell types including macrophages, Th2 cells, regulatory T cells, dendritic cells, and B

555 cells. [41] Several studies including the Leiden 85-plus study have shown that immune cells from
556 individuals with metabolic syndrome or type 2 diabetes expressed lower levels of IL-10 upon
557 stimulation. [42] While untreated HIV infection may be associated with increased expression of IL-
558 10, which in turn is thought to suppress T-cell responses. [43] Over time and with antiretroviral
559 therapy treatment, IL-10 expression decreases and may be associated with metabolic disease
560 in PWH.[44,45] Furthermore, a study looking at the effects of exercise suggests that PWH are
561 unable to increase IL-10 expression when compared to HIV-negative individuals. [46] In this study,
562 the relationship between the T cell-monocyte complexes and IL-10 and the interaction between
563 hemoglobin A1C and IL-10 reinforces the notion that complexes arise in the setting of
564 inflammation. [47] Taken together, a state of systemic inflammation in PWH, compounded with
565 diabetes and a lack of adequate inhibitory responses, could enhance the presence of the T cell-
566 monocyte immune complexes.
567
568 A recent study on immunometabolism of $CD4^+$ T cells in the context of HIV showed that the
569 infectivity of the $CD4^+$ T cells was more dependent on the metabolic activity of the T cells and
570 less on the activation status. [48,49] They separated $CD4^+$ T cells based on their metabolic activity
571 and then infected with HIV and observed a higher magnitude of HIV infection with those that
572 were more metabolically active (both oxidative phosphorylation and glycolysis). Interestingly,
573 they also showed fewer cells with latent HIV infection, when they partially inhibited glycolysis
574 using 2DG, suggesting that the steps required for HIV to establish latency are glucose
575 dependent. In our study, $CD3^+$ $CD14^+$ immune complexes were metabolically active with
576 dependence on glucose than oxidative phosphorylation. Based on the recent study, this would
577 make the T cells and possibly monocytes better able to support an HIV viral reservoir.
578 Importantly, the formation of these immune complexes is an energy-demanding process, and
579 the inhibition of oxidative phosphorylation may have been sufficient to affect some of these
580 immunological synapses as previously published. [50]

581

582 In summary, we have defined specific features of metabolically active, dynamic T cell-monocyte
583 immune complexes increased with glucose intolerance in the setting of chronic HIV infection. In
584 PWH, these cells also represent a fraction of the HIV reservoir that is likely to be recruited into
585 the tissue to establish a tissue reservoir. The complex interplay between inflammatory and
586 metabolic disorders makes these cells particularly interesting. Future studies investigating these
587 cells in vivo will provide insight into their role in the development of metabolic disease and
588 complications that may arise from this.

589

590 **Limitations of the study**

591 This is a cross-sectional study that is not able to show causality, therefore while the
592 inflammatory immune complexes are increased in persons with HIV with increased glucose
593 tolerance and appear to carry HIV, we are currently unable to make conclusions as to whether
594 these immune complexes are important in the pathogenesis of the metabolic disease. Another
595 limitation is that our conclusions cannot be extended to HIV-negative individuals at this time.
596 Future studies in mouse models and human cohorts with and without metabolic disease,
597 including PWH are needed to understand the extent to which the immune complexes may be
598 important in the pathogenesis of a metabolic disease or may be associated with complications
599 related to metabolic disease.

600

601 **STAR Methods**

KEY RESOURCES TABLE			
CYTOF Reagents			
Target	**Metal Tag**	**Tag Isotope**	**Source or reference**
CD45	Y	89	Fluidigm
CCR6	Praseodymium (Pr)	141	Fluidigm
CD57	Neodymium (Nd)	142	Fluidigm
CD127	Neodymium (Nd)	143	Fluidigm
CD38	Neodymium (Nd)	144	Fluidigm
CD4	Neodymium (Nd)	145	Fluidigm
CD8a	Neodymium (Nd)	146	Fluidigm
CD14 M5E2	Neodymium (Nd)	148	Fluidigm
CD45RO	Samarium (Sm)	149	Fluidigm
CD86	Neodymium	150	Fluidigm
ICOS	Europium (Eu)	151	Fluidigm
TCRgd	Samarium (Sm)	152	Fluidigm
CD45RA	Europium (Eu)	153	Fluidigm
GPR56	Samarium (Sm)	154	CIC core
PD-1	Gadolinium (Gd)	155	Fluidigm
CXCR3	Gadolinium (Gd)	156	Fluidigm
OX40	Gadolinium (Gd)	158	Fluidigm
CCR7	Terbium (Tb)	159	Fluidigm
CD28	Gadolinium (Gd)	160	Fluidigm
CD152/CTLA4	Dysprosium (Dy)	161	Fluidigm
FoxP3	Dysprosium (Dy)	162	Fluidigm
CRTH2	Dysprosium (Dy)	163	Fluidigm

CD161	Dysprosium (Dy)	164	Fluidigm
CD19	Holmium(Ho)	165	Fluidigm
NKG2D	Erbium (Er)	166	Fluidigm
CD27	Erbium (Er)	167	Fluidigm
CD138	Erbium (Er)	168	Fluidigm
CD25	Thulium (TM)	169	Fluidigm
CD3	Erbium (Er)	170	Fluidigm
CD20	Ytterbium (Yb)	171	Fluidigm
CX3CR1	Ytterbium (Yb)	172	CIC core
CD137	Ytterbium (Yb)	173	Fluidigm
HLA-Dr	Lutetium (Lu)	174	Fluidigm
CCR4	Lutetium (Lu)	175	Fluidigm
CD56/NCAM	Ytterbium (Yb)	176	Fluidigm
Nuc acid --Ir	Iridium (Ir)	191/193	Fluidigm
Cisplatin	Platinum (Pt)	195	Fluidigm
CD16	Bismuth (Bi)	209	Fluidigm
Flow Cytometry Reagents **BD ARIA**			
Target	**Fluorescent Tag**	**Source or Reference**	**Catalog number**
CD3 (Clone SK7)	BV786	BD Biosciences	#563800
CD4 (Clone RPA-T4)	PcPCy5.5	BD Biosciences	#560650
CD8 (Clone PRA-T8)	A700	BD Biosciences	#557945
CCR7 (Clone 150503)	BV421	BD Biosciences	#562555
CD45RO (Clone UCHL1)	PECF594	BD Biosciences	#562299
LIVE/DEAD Fixable Aqua	N/A	ThermoFisher	#L34957

CD57 (Lot 4182924)	FITC	BD Pharmingen	# 555619
CX3CR1(Clone 2A9-1)	PE	BD Biosciences	#565796
GPR56 (Clone CG4)	PECY7	BioLegend	#358205
CD14 (Clone M5E2)	APC	BD Biosciences	#561383
CD19 (Clone HIB19)	V500	BD Biosciences	#561121
CYTEK			
GPR56 (Clone 4C3)	APC	BioLegend	#391905
CCR7 (Clone G043H7)	Spark NIR 685	BioLegend	#353257
CD38 (Clone HIT2)	AF700	BD Biosciences	#560676
KLRG1 (Clone 2F1-KLRG1)	APC CY7	BioLegend	#138425
CD14 (Clone 63D3)	APC Fire 810	BioLegend	#367155
CX3CR1 (Clone 2A9-1)	PE	BD Biosciences	#565796
CD45RO (Clone UCHL1)	PE-CF594	BD Biosciences	#562299
CXCR3 (Clone G025H7)	PE-CY5	BioLegend	#353755
PD1 (Clone EH12.2H7)	PE Fire 700	BioLegend	#329918
CD27 (Clone O323)	PE-CY7	BioLegend	#302859
Puromycin AF488	PE Fire 810	Millipore,	#MABE343-AF488
CD16 PerCP	PerCP	Biolegend	#302030
L/D Zombie Violet	BB660	BioLegend	#423113
CD3 BV480 (Clone UCHT1)	BV480	BD Biosciences	#566166
CD19 BV510 (Clone HIB19)	BB510	BioLegend	#302241
CD8 BV570 (Clone RPA-T8)	BB570	BioLegend	#301037
CD4 BV650 (Clone RPA-T4)	BV650	BioLegend	#300535
CD28 BV711 (Clone CD28.2)	BV711	BioLegend	#302947
CXCR5 BV785 (Clone J252D24)	BV785	BioLegend	#356935
Energy Metabolism Profiling with SCENITH			

Anti-puromycin (Clone 12D10)	AF488	Millipore Sigma	#MABE343
Puromycin solution	N/A	Sigma Aldrich	#P8833-10MG
Oligomycin A	N/A	Sigma Aldrich	#75351-5MG
2-deoxy-D-glucose 2mM	N/A	Sigma Aldrich	#D8375
Software and Algorithms			
R 4.1.2	The R project for Statistical Computing	https://www.r-project.org/	
Cytobank Vanderbilt	Cytobank	Vanderbilt.cytobank.org	
GraphPad Prism version 9.5.0	GraphPad Software	https://www.graphpad.com	
FlowJo V	Tree Star	https://www.flowjo.com	
TCRmatch	IEDB	http://tools.iedb.org/tcrmatch/	
VGAS	IIID	https://www.iiid.com.au/software/vgas	

602

603 **Resource availability**

604 Requests for further details on protocols and data included in this study are available upon
605 request from the lead contact, celestine.wanjalla@vumc.org

606

607 **Study Participants**

608 All PWH were previously recruited for the *HIV, Adipose Tissue Immunology and Metabolism*
609 *cohort* (HATIM) at the Vanderbilt Comprehensive Care clinic from 2017 to 2020 (first visit) and
610 2021 to 2022 (second visit). The cohort was developed to study contributors to metabolic
611 disease in treated HIV infection and included individuals without diabetes (hemoglobin A1c
612 [HbA1c] <5.7% and fasting blood glucose [FBG] <100 mg/dl), with prediabetes (HbA1c 5.7-6.4%
613 and/or FBG 100-125 mg/dl), and diabetes (HbA1c ≥6.5%, FBG≥126 mg/dl and/or on

614 medications to treat diabetes). All PWH were on antiretroviral therapy with sustained viral
615 suppression for a minimum of 12 months before the study, with a $CD4^+$ T cell count > 350
616 cells/ml (**Supplemental Table 1**). The cohort excluded individuals with inflammatory illnesses,
617 substance abuse (amphetamines and cocaine), greater than 11 alcoholic drinks per week, and
618 active hepatitis B and C. The study is registered at ClinicalTrials.gov (NCT04451980) and
619 additional details are previously published. [2] This study was approved by the Vanderbilt
620 University of Medicine Institutional Review Boards. Participants in this study provided written
621 informed consent and questions answered where applicable. Records and samples are stored
622 with de-identified labels. The investigators carried out studies by the guidelines of the United
623 States Department of Health and Human Services.
624
625 **Mass cytometry**
626 Cryopreserved PBMCs were thawed in RPMI media containing Nuclease S7 (20ul). The
627 PBMCs were pelleted, washed in PBS without calcium or magnesium, and resuspended in 1ml
628 RPMI media followed by incubation with 10uM Cisplatin (3 minutes before quench with
629 RPMI/10% fetal bovine serum) to stain for LIVE/Dead cells. Cells were then washed twice with
630 PBS/1% BSA. For all 37 antibodies included in the panel, we made a master mix with the
631 surface markers (**Supplemental Table 2**). The cells were incubated with the master mix of
632 antibodies for 30 minutes at room temperature, followed by two washes with PBS, and a fix with
633 1.6% paraformaldehyde. The cells were washed two additional times with PBS and then
634 resuspended in 1ml of cold methanol and stored at -20°C. One day prior to running the samples
635 on the Helios, the cells were washed twice with PBS and resuspended in PBS/1% BSA. Cells
636 were then stained with intracellular markers (CTLA4 and FOXP3) for 20 minutes at room
637 temperature. The cells were then stained with 2ul (250nM) of DNA intercalator (Ir) in PBS with
638 1.6% PFA. Just prior to running the cells were washed in PBS followed by Millipore water. For

639 analysis, we resuspended 500,000 cells/ml of Millipore H_2O. $^1/_{10}$ volume of equilibration beads
640 were added to the cells, which were then filtered and run on the Helios.
641
642 FCS files from the Helios cytometer were bead-normalized using the premessa R package's
643 normalizer GUI method.[51] FCS files were then submitted to a gating scheme using Flowjo to
644 clean the data of debris (DNA-), Fluidigm beads (175++165++), events that showed obvious
645 doublet character by Gaussian parameters (EventLength high Residual high), and dead cells
646 (cisplatin$^+$). Using Flowjo, various cell types were targeted for analysis including CD45+
647 lymphocytes, CD4$^+$ T cells, CD8$^+$ T cells, Monocytes, B cells, and NK cells (refer to gating
648 scheme figure if appropriate). Gated subsets were exported from Flowjo for further analysis.
649 The R programming language (version 4.2.1) was used for the subsequent analysis steps.
650 CD45+ lymphocyte exports were downsampled to 40000 events per sample, CD4$^+$ T cell
651 exports were downsampled to 40000 events per sample, CD8+ T cell exports were
652 downsampled to 40000 events per sample, Monocyte exports were downsampled to 30000
653 events per sample, B cell exports were downsampled to 30000 events per sample, and NK cell
654 exports were downsampled to 30000 events per sample. All FCS file handling in R was done
655 using the flowCore package. [52] Each downsampled subset was passed through the following
656 workflow: Subset parameters were transformed using the function asinh(x/5). A nearest
657 neighbor search was done to produce a weighted adjacency matrix with a number of nearest
658 neighbors set to the dimension of subset + 1. [53] The Leiden community detection algorithm was
659 used to cluster the adjacency matrix. [54] Uniform Manifold Approximation and Projection (UMAP)
660 was done for subset visualization using the uwot R package. [55]
661
662 **Tracking Expanding populations (T-REX) and Marker Enrichment Modeling (MEM) of**
663 **enriched features**

664 The T-REX algorithm was performed as published. [23] In brief, we classified cells of interest
665 measured using mass cytometry including $CD45^+$ cells, $CD3^+$ $CD4^+$ T cells, $CD3^+$ $CD8^+$ T cells,
666 $CD3^-$ $CD19^-$ HLA-DR^+ monocytes, and $CD3^-$ $CD56^+$ $CD16^+$ NK cells. UMAP analyses were
667 performed for concatenated non-diabetic participants (group 1) and prediabetic/diabetic
668 participants (group 2). This was followed by K nearest neighbor (KNN) analyses to search for
669 the nearest neighbors for each cell. The difference in the percent change per cell between
670 group 1 and group 2 is calculated based on the abundance of these cells in each group in the
671 KNN region. ≤5% and ≥95% changes in cell percentages were considered significant, which we
672 clustered using DBSCAN. The phenotype of the clusters that were significantly different
673 between the groups was determined using the MEM package.
674
675 **Flow cytometry**
676 PBMCs were stained with fluorescently tagged antibodies as previously published. [20] In brief,
677 thawed and washed PBMCs were stained with Aqua (Live/Dead marker) for 10 minutes at room
678 temperature, followed by the addition of fluorescently tagged antibodies against T cells [CD3-
679 BV786, CD4-PerpCP cy5.5, CD8-A700], monocytes [CD14-APC], T-cell memory subsets
680 [CD45RO and CCR7]. CD19 antibody was included in the Aqua channel (therefore we did not
681 evaluate CD19 cells for flow cytometry). For the SCENITH assay, we used antibodies [anti-
682 puromycin, Zombie, CD3, CD4, CD8, CD14, CD16, CD19, CD27, CD28, CD38, CCR7,
683 CD45RO, CX3CR1, CXCR3, PD1, CXCR5, IgD, and KLRG1).
684
685 **Droplet digital PCR**
686 We sorted $CD3^+$ $CD4^+$ T cells, $CD14^+$ monocytes, and $CD3^+$ $CD14^+$ T cell-monocyte complexes
687 into separate Eppendorf tubes with PBS. Cells were pelleted and resuspended in lysis buffer
688 [Tritonx100 (0.1%), Tris HCL (10mM), and Proteinase K (400ug/ml)] at 55°C for 10 hours.
689 Additional proteinase K was added during the heat inactivation stage at 95°C for 5 minutes. For

690 HIV DNA quantitation, we used LTR primers (LTR 5'AGC ACT CAA GGC AAG CTT TA-3', and
691 reverse primer -LTR 5' TGT ACT GGG TCT CTC TGG TTA G-3', and probe 5'-FAM-GCA GTG
692 GGT TCC CTA GTT AGC CAG AGA G-3IABkFQ3'). [56] HIV transcripts were quantified as
693 copies/million cells. 19ul of the ddPCR SuperMix (LTR primers & RPP30 housekeeping
694 gene primers and probes), and 6ul of cell lysates were mixed and aliquoted per well (96-well
695 twin tec plate) and droplets generated with an AutoDG. Droplets were read using a plate reader,
696 and the positive droplet threshold was manually set using the negative droplet control (media
697 only).
698
699 **Single-cell T-cell receptor (TCR) sequencing**
700 We sequenced TCRs from single cells as previously published. [57] In brief, we index sorted
701 single $CD3^+$ $CD14^+$ T cell-monocyte complexes into 96 well plates with 3μL of lysis buffer. We
702 used primers with uniquely tagged barcodes with a unique molecular identifier (UMI) for reverse
703 transcription. This allowed for multiplexing. cDNA was pooled and amplified using the KAPA
704 HiFi HotStart ReadyMix (Roche, Basel, Switzerland), as per the manufacturer's instructions. We
705 quantified individual TCR gene expression using the UMIs [58-60]. Nested PCRs were done
706 targeting the TCR. 2μL of pooled cDNA was enriched for TCRab genes using the TSOend
707 primer and the constant region primers, TCRA or TCRB. These products were purified and
708 pooled. We created indexed libraries for sequencing using Truseq adapters and quantified using
709 the Jetseq qPCR Library Quantification Kit (Meridian Biosciences Inc., OH, USA), as per the
710 manufacturer's instructions. We sequenced samples on an Illumina MiSeq using a 2×300bp
711 paired-end chemistry kit (Illumina Inc., CA, USA). Sequencing reads were quality-filtered and
712 demultiplexed to assign reads to individual wells and sequences mapped to the TCRA and
713 TCRB loci and assigned TCR clonotypes using the MIXCR software. [61] Circos plots were
714 generated using the visual genomics analysis studio (VGAS).[62]
715

716 **Time-lapse imaging**

717 $CD3^+$ $CD14^+$ T cell-monocyte complexes were sorted as above and resuspended in RPMI with
718 10% fetal bovine serum (FBS). The cells were then plated on poly-L-Lysine pre-coated
719 coverslips at a density of 15,000 -40,000 complexes per 100 μl media. The cells on the
720 coverslip were placed in a 24-well plate and time-lapse imaging was captured using an EVOS
721 M5000 imaging system. Image J Version 1.53t 24 August 2022 was used for image analysis.

722

723 **Transmission electron microscopy**

724 $CD3^+$ $CD14^+$ T cell-monocyte complexes, $CD3^+$ $CD4^+$ T cells, and $CD14^+$ monocytes were sorted
725 as above and plated on poly-L-Lysine pre-coated coverslips. For day 3 samples, we added RPMI
726 media supplemented with human IL-2 [10ng/mL]. For doublet imaging, the cells were plated on a
727 poly-L-lysine coated coverslip for 1-2 hours. Then when the cells are bound to the coverslip, the
728 media was aspirated and then the cells were fixed with 2.5% glutaraldehyde solution in 0.1 M
729 sodium cacodylate buffer. [63] After secondary fixation, samples were washed for five mins with
730 0.1 M sodium cacodylate buffer (7.3 pH). From there, we performed two washes of five mins with
731 diH_2O to ensure the plates were cleaned. While keeping all solutions and plates at room
732 temperature, the samples were incubated with 2.5% uranyl acetate, diluted with H_2O, at 4 °C
733 overnight. Following this, samples were dehydrated using an ethanol gradient series. After
734 dehydration, the ethanol was replaced with Eponate 12™ mixed in 100% ethanol in a 1:1 solution,
735 then incubated at room temperature for 30 mins. This was repeated three times for 1 hour using
736 100% Eponate 12™.

737

738 The plates were finally placed in new media and cured in an oven at 70 °C overnight. The plates
739 were cracked upon hardening, and the cells were separated by submerging the plate in liquid
740 nitrogen. An 80 nm thickness jeweler's saw was used to cut the block to fit in a Leica UC6
741 ultramicrotome sample holder. The section was placed on formvar-coated copper grids

742 counterstained in 2% uranyl acetate for 2 mins. Then the grids were counterstained by Reynold's
743 lead citrate for two mins. Images were acquired by TEM on either a JEOL JEM-1230, operating
744 at 120 kV, or a JEOL 1400, operating at 80 kV. [64]
745
746 **Single-cell RNA sequencing**
747 We performed 10X sequencing on PBMCs from one prediabetic participant with a significant
748 proportion of $CD3^+$ $CD14^+$ T cell-monocyte complexes as determined by flow cytometry. PBMCs
749 were thawed and washed with PBS (no calcium or magnesium), and the pellet was
750 resuspended in 100µL of cell staining buffer. The cells were incubated with Fc receptor-blocking
751 solution (5 µL, TruStain). Cells were incubated on ice for 10 minutes. A Total Seq C master mix
752 containing surface antibodies (CD3 clone UCHT1 #300479, CD4 clone SK3 #344651, CD8a
753 clone SK1 #344753, CD14 clone 63D3 #367137, CD16 clone 3G8 #302065, CD69 clone FN50
754 #310951) was prepared. 3µL of the master mix was added to each sample, which was
755 incubated on ice for 30 minutes. The cells were washed three times and resuspended in 0.04%
756 BSA in PBS. We submitted twenty thousand cells that were loaded onto the Chromium Single
757 Cell 5' assay (10x Genomics). Cells were encapsulated and feature barcoded, with library
758 preparation, cDNA amplification, and sequencing (50bp paired-end reads, on NovaSeq 6000 S2
759 platform). We aligned the raw sequencing reads to the human genome (hg38) using STAR
760 v.2.7.2a. We identified cells using cell ranger (version 7.1). Downstream analysis was
761 performed using the Seurat V4. [65] We filtered out cells with ≤ 200 genes, umi ≤ 400 or > 4000,
762 and ≤ 10% mitochondrial genes expressed. We used DoubletFinder with default settings to
763 identify heterotypic doublets. We then performed downstream analyses on the RNA count
764 matrix including feature selection, scaling and centering counts, principal component analysis,
765 Uniform Manifold Approximation, and Projection (UMAP) reduction, shared nearest neighbor
766 graph construction, and finally cluster determination. Annotation was performed using cell-

767 specific gene markers. Doublets were identified by the expression of multiple cell lineages and
768 confirmed by DoubletFinder classification.
769
770 **Statistical analysis**
771 Statistical analysis in this study was performed in Graph pad Prism version 9.5.0 and R version
772 4.2.1.
773
774 **Data and code availability**
775 Gene expression data from this study have been deposited in the NIH Gene Expression
776 Omnibus (GEO) accession numbers: GSE229707 and GSE230276.
777
778 **Acknowledgments**
779 The graphical abstract was created using BioRender.
780
781 **Author Contributions**
782 Conceptualization, C.N.W., J.R.K.; Methodology, C.N.W., J.S., J. O., X.Z., M.M., S.A.M., H.B.,
783 A. H., E.W., S.A.K., T.T., C.L.G., D.G.H., E.J.P., J.R.K.; Statistics, C.N.W., J.S., J.R.K.; Formal
784 Analysis, C.N.W., J.S., J.O., C.M.W., R.G., A.C., S.P. ; Investigation, C.N.W., C.M.W., J.R.K;
785 Resources, J.R.K., S.A.K.; Data Curation, C.N.W., S.B., Q.S., J.S., J. R. K.; Writing – Original
786 Draft, C.N.W.; Writing – Review & Editing original draft., C.N.W., J.S., J. O., X.Z., M.M., S.A.M.,
787 H.B., A. H., E.W., S.A.K., T.T., D.G.H., E.J.P., J.R.K.; Visualization, C.N.W., S.P., J.W., S.B.,
788 Q.S., J.S., H.B., A.H.; Supervision, C.N.W, J.R.K., Project Administration, C.N.W., J.R.K.;
789 Funding Acquisition, C.N.W., J.R.K.
790
791 **Acknowledgments**

792 Doris Duke CSDA 2021193 (CNW), K23 HL156759 (CNW), Burroughs Wellcome Fund
793 1021480 (CNW), R01 DK112262 (JRK), the Tennessee Center for AIDS Research grant P30
794 AI110527 (SAM), KL2TR002245 (MM and EMW), K08AR080808 (EMW), The Myositis
795 Association Pilot Award Grant (EMW), the Vanderbilt Flow Cytometry Shared Resource is
796 supported by the Vanderbilt Ingram Cancer Center (P30 CA068485) and the Vanderbilt
797 Digestive Disease Research Center (DK058404).
798

799 **Declaration of interests**

800 The authors have no competing interests.

801 **References**

802 1. Bailin, S.S., Kundu, S., Wellons, M., Freiberg, M.S., Doyle, M.F., Tracy, R.P., Justice, A.C.,
803 Wanjalla, C.N., Landay, A.L., So-Armah, K., et al. (2022). Circulating CD4+ TEMRA and
804 CD4+ CD28- T cells and incident diabetes among persons with and without HIV. Aids *36*,
805 501-511. 10.1097/qad.0000000000003137.
806 2. Wanjalla, C.N., Mashayekhi, M., Bailin, S., Gabriel, C.L., Meenderink, L.M., Temu, T.,
807 Fuller, D.T., Guo, L., Kawai, K., Virmani, R., et al. (2021). Anticytomegalovirus CD4 $^{+}$ T
808 Cells Are Associated With Subclinical Atherosclerosis in Persons With HIV. Arterioscler
809 Thromb Vasc Biol *Apr;41(4):1459-1473.*, ATVBAHA120315786.
810 10.1161/ATVBAHA.120.315786.
811 3. Bailin, S.S., McGinnis, K.A., McDonnell, W.J., So-Armah, K., Wellons, M., Tracy, R.P.,
812 Doyle, M.F., Mallal, S., Justice, A.C., Freiberg, M.S., et al. (2020). T Lymphocyte Subsets
813 Associated with Prevalent Diabetes in Veterans with and without HIV. J Infect Dis.
814 10.1093/infdis/jiaa069.
815 4. Kundu, S., Freiberg, M.S., Tracy, R.P., So-Armah, K.A., Koethe, J.R., Duncan, M.S., Tindle,
816 H.A., Beckman, J.A., Feinstein, M.J., McDonnell, W.J., et al. (2022). Circulating T Cells and
817 Cardiovascular Risk in People With and Without HIV Infection. J Am Coll Cardiol *80*,
818 1633-1644. 10.1016/j.jacc.2022.08.756.
819 5. Temu, T.M., Polyak, S.J., Zifodya, J.S., Wanjalla, C.N., Koethe, J.R., Masyuko, S.,
820 Nyabiage, J., Kinuthia, J., Gervassi, A.L., Oyugi, J., et al. (2020). Endothelial Dysfunction Is
821 Related to Monocyte Activation in Antiretroviral-Treated People With HIV and HIV-
822 Negative Adults in Kenya. Open forum infectious diseases *7*, ofaa425.
823 10.1093/ofid/ofaa425.
824 6. Temu, T.M., Wagoner, J., Masyuko, S., O'Connor, A., Zifodya, J.S., Macharia, P., Wanjalla,
825 C.N., Mogaka, J.N., Chohan, B., Omodi, V.M., et al. (2021). Central obesity is a
826 contributor to systemic inflammation and monocyte activation in virally suppressed
827 adults with chronic HIV in Kenya. AIDS *35*, 1723-1731.
828 10.1097/QAD.0000000000002956.
829 7. Alcaide, M.L., Parmigiani, A., Pallikkuth, S., Roach, M., Freguja, R., Della Negra, M.,
830 Bolivar, H., Fischl, M.A., and Pahwa, S. (2013). Immune activation in HIV-infected aging
831 women on antiretrovirals--implications for age-associated comorbidities: a cross-
832 sectional pilot study. PLoS One *8*, e63804. 10.1371/journal.pone.0063804.
833 8. Grome, H.N., Barnett, L., Hagar, C.C., Harrison, D.G., Kalams, S.A., and Koethe, J.R.
834 (2017). Association of T Cell and Macrophage Activation with Arterial Vascular Health in
835 HIV. AIDS Res Hum Retroviruses *33*, 181-186. 10.1089/AID.2016.0113.
836 9. Hsue, P.Y., and Waters, D.D. (2019). HIV infection and coronary heart disease:
837 mechanisms and management. Nat Rev Cardiol *16*, 745-759. 10.1038/s41569-019-0219-
838 9.
839 10. Staats, J., Divekar, A., McCoy, J.P., and Maecker, H.T. (2019). Guidelines for Gating Flow
840 Cytometry Data for Immunological Assays. Methods Mol Biol *2032*, 81-104.
841 10.1007/978-1-4939-9650-6_5.

842 11. Guo, R., Lü, M., Cao, F., Wu, G., Gao, F., Pang, H., Li, Y., Zhang, Y., Xing, H., Liang, C., et al.
843 (2021). Single-cell map of diverse immune phenotypes in the acute myeloid leukemia
844 microenvironment. Biomark Res *9*, 15. 10.1186/s40364-021-00265-0.
845 12. Lloyd, M.G., Smith, N.A., Tighe, M., Travis, K.L., Liu, D., Upadhyaya, P.K., Kinchington,
846 P.R., Chan, G.C., and Moffat, J.F. (2020). A Novel Human Skin Tissue Model To Study
847 Varicella-Zoster Virus and Human Cytomegalovirus. J Virol *94*. 10.1128/JVI.01082-20.
848 13. Burel, J.G., Pomaznoy, M., Lindestam Arlehamn, C.S., Weiskopf, D., da Silva Antunes, R.,
849 Jung, Y., Babor, M., Schulten, V., Seumois, G., Greenbaum, J.A., et al. (2019). Circulating
850 T cell-monocyte complexes are markers of immune perturbations. Elife *8*.
851 10.7554/eLife.46045.
852 14. Gil-Manso, S., Miguens Blanco, I., López-Esteban, R., Carbonell, D., López-Fernández,
853 L.A., West, L., Correa-Rocha, R., and Pion, M. (2021). Comprehensive Flow Cytometry
854 Profiling of the Immune System in COVID-19 Convalescent Individuals. Front Immunol
855 *12*, 793142. 10.3389/fimmu.2021.793142.
856 15. Sivakumar, S., Abu-Shah, E., Ahern, D.J., Arbe-Barnes, E.H., Jainarayanan, A.K., Mangal,
857 N., Reddy, S., Rendek, A., Easton, A., Kurz, E., et al. (2021). Activated Regulatory T-Cells,
858 Dysfunctional and Senescent T-Cells Hinder the Immunity in Pancreatic Cancer. Cancers
859 (Basel) *13*. 10.3390/cancers13081776.
860 16. Burel, J.G., Pomaznoy, M., Lindestam Arlehamn, C.S., Seumois, G., Vijayanand, P., Sette,
861 A., and Peters, B. (2020). The Challenge of Distinguishing Cell-Cell Complexes from
862 Singlet Cells in Non-Imaging Flow Cytometry and Single-Cell Sorting. Cytometry A *97*,
863 1127-1135. 10.1002/cyto.a.24027.
864 17. Henry, C., Ramadan, A., Montcuquet, N., Pallandre, J.R., Mercier-Letondal, P.,
865 Deschamps, M., Tiberghien, P., Ferrand, C., and Robinet, E. (2010). CD3+CD20+ cells may
866 be an artifact of flow cytometry: comment on the article by Wilk et al. Arthritis Rheum
867 *62*, 2561-2563; author reply 2563-2565. 10.1002/art.27527.
868 18. Clayton, K.L., Collins, D.R., Lengieza, J., Ghebremichael, M., Dotiwala, F., Lieberman, J.,
869 and Walker, B.D. (2018). Resistance of HIV-infected macrophages to CD8. Nat Immunol
870 *19*, 475-486. 10.1038/s41590-018-0085-3.
871 19. Jenkins, M.R., Rudd-Schmidt, J.A., Lopez, J.A., Ramsbottom, K.M., Mannering, S.I.,
872 Andrews, D.M., Voskoboinik, I., and Trapani, J.A. (2015). Failed CTL/NK cell killing and
873 cytokine hypersecretion are directly linked through prolonged synapse time. J Exp Med
874 *212*, 307-317. 10.1084/jem.20140964.
875 20. Wanjalla, C.N., McDonnell, W.J., Barnett, L., Simmons, J.D., Furch, B.D., Lima, M.C.,
876 Woodward, B.O., Fan, R., Fei, Y., Baker, P.G., et al. (2019). Adipose Tissue in Persons
877 With HIV Is Enriched for CD4. Front Immunol *10*, 408. 10.3389/fimmu.2019.00408.
878 21. Wanjalla, C.N., McDonnell, W.J., Ram, R., Chopra, A., Gangula, R., Leary, S., Mashayekhi,
879 M., Simmons, J.D., Warren, C.M., Bailin, S., et al. (2021). Single-cell analysis shows that
880 adipose tissue of persons with both HIV and diabetes is enriched for clonal, cytotoxic,
881 and CMV-specific CD4+ T cells. Cell Rep Med *2*, 100205. 10.1016/j.xcrm.2021.100205.
882 22. Diggins, K.E., Greenplate, A.R., Leelatian, N., Wogsland, C.E., and Irish, J.M. (2017).
883 Characterizing cell subsets using marker enrichment modeling. Nat Methods *14*, 275-
884 278. 10.1038/nmeth.4149.

885 23. Barone, S.M., Paul, A.G., Muehling, L.M., Lannigan, J.A., Kwok, W.W., Turner, R.B.,
886 Woodfolk, J.A., and Irish, J.M. (2021). Unsupervised machine learning reveals key
887 immune cell subsets in COVID-19, rhinovirus infection, and cancer therapy. Elife *10*.
888 10.7554/eLife.64653.
889 24. Hotamisligil, G.S. (2006). Inflammation and metabolic disorders. Nature *444*, 860-867.
890 10.1038/nature05485.
891 25. Groot, F., Welsch, S., and Sattentau, Q.J. (2008). Efficient HIV-1 transmission from
892 macrophages to T cells across transient virological synapses. Blood *111*, 4660-4663.
893 10.1182/blood-2007-12-130070.
894 26. Parry, H.M., Zuo, J., Frumento, G., Mirajkar, N., Inman, C., Edwards, E., Griffiths, M.,
895 Pratt, G., and Moss, P. (2016). Cytomegalovirus viral load within blood increases
896 markedly in healthy people over the age of 70 years. Immun Ageing *13*, 1.
897 10.1186/s12979-015-0056-6.
898 27. Palmer, C.S., Cherry, C.L., Sada-Ovalle, I., Singh, A., and Crowe, S.M. (2016). Glucose
899 Metabolism in T Cells and Monocytes: New Perspectives in HIV Pathogenesis.
900 EBioMedicine *6*, 31-41. 10.1016/j.ebiom.2016.02.012.
901 28. O'Neill, L.A., Kishton, R.J., and Rathmell, J. (2016). A guide to immunometabolism for
902 immunologists. Nat Rev Immunol *16*, 553-565. 10.1038/nri.2016.70.
903 29. Randolph, G.J., Beaulieu, S., Lebecque, S., Steinman, R.M., and Muller, W.A. (1998).
904 Differentiation of monocytes into dendritic cells in a model of transendothelial
905 trafficking. Science *282*, 480-483. 10.1126/science.282.5388.480.
906 30. Lambotte, O., Taoufik, Y., de Goër, M.G., Wallon, C., Goujard, C., and Delfraissy, J.F.
907 (2000). Detection of infectious HIV in circulating monocytes from patients on prolonged
908 highly active antiretroviral therapy. J Acquir Immune Defic Syndr *23*, 114-119.
909 10.1097/00126334-200002010-00002.
910 31. Zhu, T., Muthui, D., Holte, S., Nickle, D., Feng, F., Brodie, S., Hwangbo, Y., Mullins, J.I.,
911 and Corey, L. (2002). Evidence for human immunodeficiency virus type 1 replication in
912 vivo in CD14(+) monocytes and its potential role as a source of virus in patients on highly
913 active antiretroviral therapy. J Virol *76*, 707-716. 10.1128/jvi.76.2.707-716.2002.
914 32. McElrath, M.J., Steinman, R.M., and Cohn, Z.A. (1991). Latent HIV-1 infection in enriched
915 populations of blood monocytes and T cells from seropositive patients. J Clin Invest *87*,
916 27-30. 10.1172/JCI114981.
917 33. Sonza, S., Mutimer, H.P., Oelrichs, R., Jardine, D., Harvey, K., Dunne, A., Purcell, D.F.,
918 Birch, C., and Crowe, S.M. (2001). Monocytes harbour replication-competent, non-latent
919 HIV-1 in patients on highly active antiretroviral therapy. AIDS *15*, 17-22.
920 10.1097/00002030-200101050-00005.
921 34. Ellery, P.J., Tippett, E., Chiu, Y.L., Paukovics, G., Cameron, P.U., Solomon, A., Lewin, S.R.,
922 Gorry, P.R., Jaworowski, A., Greene, W.C., et al. (2007). The CD16+ monocyte subset is
923 more permissive to infection and preferentially harbors HIV-1 in vivo. J Immunol *178*,
924 6581-6589.
925 35. Carr, J.M., Hocking, H., Li, P., and Burrell, C.J. (1999). Rapid and efficient cell-to-cell
926 transmission of human immunodeficiency virus infection from monocyte-derived
927 macrophages to peripheral blood lymphocytes. Virology *265*, 319-329.
928 10.1006/viro.1999.0047.

929 36. Crowe, S., Zhu, T., and Muller, W.A. (2003). The contribution of monocyte infection and
930 trafficking to viral persistence, and maintenance of the viral reservoir in HIV infection. J
931 Leukoc Biol *74*, 635-641. 10.1189/jlb.0503204.
932 37. Busman-Sahay, K., Starke, C.E., Nekorchuk, M.D., and Estes, J.D. (2021). Eliminating HIV
933 reservoirs for a cure: the issue is in the tissue. Curr Opin HIV AIDS *16*, 200-208.
934 10.1097/COH.0000000000000688.
935 38. Butt, A.A., McGinnis, K., Rodriguez-Barradas, M.C., Crystal, S., Simberkoff, M., Goetz,
936 M.B., Leaf, D., Justice, A.C., and Study, V.A.C. (2009). HIV infection and the risk of
937 diabetes mellitus. AIDS *23*, 1227-1234. 10.1097/QAD.0b013e32832bd7af.
938 39. Brown, T.T., Cole, S.R., Li, X., Kingsley, L.A., Palella, F.J., Riddler, S.A., Visscher, B.R.,
939 Margolick, J.B., and Dobs, A.S. (2005). Antiretroviral therapy and the prevalence and
940 incidence of diabetes mellitus in the multicenter AIDS cohort study. Arch Intern Med
941 *165*, 1179-1184. 10.1001/archinte.165.10.1179.
942 40. Donath, M.Y., and Shoelson, S.E. (2011). Type 2 diabetes as an inflammatory disease.
943 Nat Rev Immunol *11*, 98-107. 10.1038/nri2925.
944 41. Moore, K.W., de Waal Malefyt, R., Coffman, R.L., and O'Garra, A. (2001). Interleukin-10
945 and the interleukin-10 receptor. Annu Rev Immunol *19*, 683-765.
946 10.1146/annurev.immunol.19.1.683.
947 42. van Exel, E., Gussekloo, J., de Craen, A.J., Frölich, M., Bootsma-Van Der Wiel, A.,
948 Westendorp, R.G., and Study, L.P. (2002). Low production capacity of interleukin-10
949 associates with the metabolic syndrome and type 2 diabetes : the Leiden 85-Plus Study.
950 Diabetes *51*, 1088-1092. 10.2337/diabetes.51.4.1088.
951 43. Brockman, M.A., Kwon, D.S., Tighe, D.P., Pavlik, D.F., Rosato, P.C., Sela, J., Porichis, F., Le
952 Gall, S., Waring, M.T., Moss, K., et al. (2009). IL-10 is up-regulated in multiple cell types
953 during viremic HIV infection and reversibly inhibits virus-specific T cells. Blood *114*, 346-
954 356. 10.1182/blood-2008-12-191296.
955 44. Werede, A.T., Terry, J.G., Nair, S., Temu, T.M., Shepherd, B.E., Bailin, S.S., Mashayekhi,
956 M., Gabriel, C.L., Lima, M., Woodward, B.O., et al. (2022). Mean Coronary Cross-
957 Sectional Area as a Measure of Arterial Remodeling Using Noncontrast CT Imaging in
958 Persons With HIV. J Am Heart Assoc *11*, e025768. 10.1161/JAHA.122.025768.
959 45. Fourman, L.T., Saylor, C.F., Cheru, L., Fitch, K., Looby, S., Keller, K., Robinson, J.A.,
960 Hoffmann, U., Lu, M.T., Burdo, T., and Lo, J. (2020). Anti-Inflammatory Interleukin 10
961 Inversely Relates to Coronary Atherosclerosis in Persons With Human Immunodeficiency
962 Virus. J Infect Dis *221*, 510-515. 10.1093/infdis/jiz254.
963 46. Erlandson, K.M., Wilson, M.P., MaWhinney, S., Rapaport, E., Liu, J., Wilson, C.C.,
964 Rahkola, J.T., Janoff, E.N., Brown, T.T., Campbell, T.B., and Jankowski, C.M. (2021). The
965 Impact of Moderate or High-Intensity Combined Exercise on Systemic Inflammation
966 Among Older Persons With and Without HIV. J Infect Dis *223*, 1161-1170.
967 10.1093/infdis/jiaa494.
968 47. de Waal Malefyt, R., Abrams, J., Bennett, B., Figdor, C.G., and de Vries, J.E. (1991).
969 Interleukin 10(IL-10) inhibits cytokine synthesis by human monocytes: an autoregulatory
970 role of IL-10 produced by monocytes. J Exp Med *174*, 1209-1220.
971 10.1084/jem.174.5.1209.

48. Valle-Casuso, J.C., Angin, M., Volant, S., Passaes, C., Monceaux, V., Mikhailova, A., Bourdic, K., Avettand-Fenoel, V., Boufassa, F., Sitbon, M., et al. (2019). Cellular Metabolism Is a Major Determinant of HIV-1 Reservoir Seeding in CD4. Cell Metab *29*, 611-626.e615. 10.1016/j.cmet.2018.11.015.
49. Taylor, H.E., and Palmer, C.S. (2020). CD4 T Cell Metabolism Is a Major Contributor of HIV Infectivity and Reservoir Persistence. Immunometabolism *2*. 10.20900/immunometab20200005.
50. Bonifaz, L., Cervantes-Silva, M., Ontiveros-Dotor, E., López-Villegas, E., and Sánchez-García, F. (2014). A Role For Mitochondria In Antigen Processing And Presentation. Immunology *144*, 461-471. 10.1111/imm.12392.
51. Gherardini, F. (2022). Premessa: R package for pre-processing of flow and mass cytometry data. https://github.com/ParkerICI/premessa.
52. Ellis B, H.P., Hahne F, Le Meur N, Gopalakrishnan N, Spidlen J, Jiang M, Finak G (2022). FlowCore: flowCore: Basic structures for flow cytometry data_. R package version 2.8.0. https://github.com/RGLab/flowCore.
53. Arya S, M.D., Kemp SE, Jefferis G (2019). RANN: Fast Nearest Neighbour Search (Wraps ANN Library) Using L2 Metric. R package version 2.6.1. https://github.com/jefferislab/RANN.
54. Kelly, S.T. (2020). Leiden: R implementation of the Leiden algorithm. R package version 0.4.3 2022 R package version 0.4.3. https://github.com/TomKellyGenetics/leiden.
55. J, M. (2022). Uwot: The Uniform Manifold Approximation and Projection (UMAP) Method for Dimensionality Reduction_. R package version 0.1.14. https://github.com/jlmelville/uwot.
56. Abana, C.O., Pilkinton, M.A., Gaudieri, S., Chopra, A., McDonnell, W.J., Wanjalla, C., Barnett, L., Gangula, R., Hager, C., Jung, D.K., et al. (2017). Cytomegalovirus (CMV) Epitope-Specific CD4(+) T Cells Are Inflated in HIV(+) CMV(+) Subjects. J Immunol *199*, 3187-3201. 10.4049/jimmunol.1700851.
57. Wanjalla, C.N., McDonnell, W.J., Ram, R., Chopra, A., Gangula, R., Leary, S., Mashayekhi, M., Simmons, J.D., Warren, C.M., Bailin, S., et al. (2021). Single-cell analysis shows that adipose tissue of persons with both HIV and diabetes is enriched for clonal, cytotoxic, and CMV-specific CD4+ T cells. Cell Rep Med *2*, 100205. 10.1016/j.xcrm.2021.100205.
58. Islam, S., Zeisel, A., Joost, S., La Manno, G., Zajac, P., Kasper, M., Lönnerberg, P., and Linnarsson, S. (2014). Quantitative single-cell RNA-seq with unique molecular identifiers. Nat Methods *11*, 163-166. 10.1038/nmeth.2772.
59. Kivioja, T., Vähärautio, A., Karlsson, K., Bonke, M., Enge, M., Linnarsson, S., and Taipale, J. (2011). Counting absolute numbers of molecules using unique molecular identifiers. Nat Methods *9*, 72-74. 10.1038/nmeth.1778.
60. Grün, D., Kester, L., and van Oudenaarden, A. (2014). Validation of noise models for single-cell transcriptomics. Nat Methods *11*, 637-640. 10.1038/nmeth.2930.
61. Bolotin, D.A., Poslavsky, S., Mitrophanov, I., Shugay, M., Mamedov, I.Z., Putintseva, E.V., and Chudakov, D.M. (2015). MiXCR: software for comprehensive adaptive immunity profiling. Nat Methods *12*, 380-381. 10.1038/nmeth.3364.

1014 62. Hertzman, R.J., Deshpande, P., Leary, S., Li, Y., Ram, R., Chopra, A., Cooper, D., Watson,
1015 M., Palubinsky, A.M., Mallal, S., et al. (2021). Visual Genomics Analysis Studio as a Tool
1016 to Analyze Multiomic Data. Front Genet *12*, 642012. 10.3389/fgene.2021.642012.
1017 63. Neikirk, K., Vue, Z., Katti, P., Rodriguez, B.I., Omer, S., Shao, J., Christensen, T., Garza
1018 Lopez, E., Marshall, A., Palavicino-Maggio, C.B., et al. (2023). Systematic Transmission
1019 Electron Microscopy-Based Identification and 3D Reconstruction of Cellular Degradation
1020 Machinery. Adv Biol (Weinh), e2200221. 10.1002/adbi.202200221.
1021 64. Lam, J., Katti, P., Biete, M., Mungai, M., AshShareef, S., Neikirk, K., Garza Lopez, E., Vue,
1022 Z., Christensen, T.A., Beasley, H.K., et al. (2021). A Universal Approach to Analyzing
1023 Transmission Electron Microscopy with ImageJ. Cells *10*. 10.3390/cells10092177.
1024 65. Hao, Y., Hao, S., Andersen-Nissen, E., Mauck, W.M., Zheng, S., Butler, A., Lee, M.J., Wilk,
1025 A.J., Darby, C., Zager, M., et al. (2021). Integrated analysis of multimodal single-cell data.
1026 Cell *184*, 3573-3587.e3529. 10.1016/j.cell.2021.04.048.
1027